Macrophage-Mediated Interleukin-6 Signaling Drives Ryanodine Receptor-2 Calcium Leak in Postoperative Atrial Fibrillation

Joshua A. Keefe[1,2], Yuriana Aguilar-Sanchez[1,2], J. Alberto Navarro-Garcia[1,2], Isabelle Ong[1,2], Luge Li[3], Amelie Paasche[1,2,4], Issam Abu-Taha[5], Marcel Tekook[4], Florian Bruns[5], Shuai Zhao[1,2], Markus Kamler[6], H. Ying Shen[7], Mihail G. Chelu[1,8,9], Na Li[1,3], Dobromir Dobrev[2,5,10], Xander H. T. Wehrens[1,2,3,11,12,13]

[1]Cardiovascular Research Institute, [2]Department of Integrative Physiology, [3]Department of Medicine, Baylor College of Medicine, Houston, TX 77030, USA.

[4]Department of Cardiology, Angiology and Pneumology, University Hospital Heidelberg, 69120 Heidelberg, Germany.

[5]Institute of Pharmacology, West German Heart and Vascular Center, University Duisburg-Essen, 45147 Essen, Germany.

[6]Department of Thoracic and Cardiovascular Surgery, West German Heart and Vascular Center Essen, University Hospital Essen, 45122 Essen, Germany.

[7]Department of Surgery, Division of Cardiothoracic Surgery, Baylor College of Medicine, Houston, TX 77030, USA.

[8]Department of Internal Medicine, Division of Cardiology, Baylor College of Medicine, Houston, TX 77030, USA.

[9]Texas Heart Institute at Baylor St. Luke's Medical Center, Houston, TX 77030, USA.

[10]Department of Medicine, Montreal Heart Institute and Université de Montréal, Montreal, Quebec, Canada.

[11]Department of Neuroscience, [12]Department of Pediatrics, [13]Center for Space Medicine, Baylor College of Medicine, Houston, TX 77030, USA.

Conflict-of-interest: The authors have declared that no conflict of interest exists.

Correspondence to: Xander Wehrens, M.D., Ph.D., Cardiovascular Research Institute, Baylor College of Medicine, BCM335, One Baylor Plaza, Houston, TX 77030. Email: wehrens@bcm.edu; ORCID:

0 0000-0001-5044-672X

1

ABSTRACT

Postoperative atrial fibrillation (poAF) is AF occurring days after surgery with a prevalence of 33% among patients undergoing open-heart surgery. The degree of postoperative inflammation correlates with poAF risk, but less is known about the cellular and molecular mechanisms driving postoperative atrial arrhythmogenesis. We performed single-cell RNA sequencing comparing atrial non-myocytes from mice with versus without poAF, which revealed infiltrating $CCR2^{+}$ macrophages to be the most altered cell type. Pseudotime trajectory analyses identified *Il-6* as a top gene in macrophages, which we confirmed in pericardial fluid collected from human patients after cardiac surgery. Indeed, macrophage depletion and macrophage-specific *Il6ra* conditional knockout (cKO) prevented poAF in mice. Downstream STAT3 inhibition with TTI-101 and cardiomyocyte-specific *Stat3* cKO rescued poAF, indicating a pro-arrhythmogenic role of STAT3 in poAF development. Confocal imaging in isolated atrial cardiomyocytes (ACMs) uncovered a novel link between STAT3 and CaMKII-mediated ryanodine receptor-2 (RyR2)-Ser(S)2814 phosphorylation. Indeed, non-phosphorylatable $RyR2^{S2814A}$ mice were protected from poAF, and CaMKII inhibition prevented arrhythmogenic Ca^{2+} mishandling in ACMs from mice with poAF. Altogether, we provide multiomic, biochemical, and functional evidence from mice and humans that IL-6-STAT3-CaMKII signaling driven by infiltrating atrial macrophages is a pivotal driver of poAF that portends therapeutic utility for poAF prevention.

Abbreviations

ACM	Atrial cardiomyocyte
Ca^{2+}	Calcium ion
CaMKII	Calcium/calmodulin-dependent protein kinase II
dPCR	Digital polymerase chain reaction
gp130	glycoprotein 130
IL-6	Interleukin-6
IL-6Rα	Interleukin-6 receptor alpha
NLRP3	NOD-, LRR-, and pyrin domain-containing protein 3
PES	Programmed electrical stimulation
poAF	Postoperative atrial fibrillation
RT-qPCR	Real-time quantitative polymerase chain reaction
RyR2	Ryanodine receptor type-2
scRNAseq	Single-cell RNA sequencing
SERCA2a	Sarco/endoplasmic reticulum ATPase 2a
Sh	Sham
SR	Sarcoplasmic reticulum
STAT3	Signal transducer and activator of transcription 3
TAF	Thoracotomy atrial fibrillation
TSR	Thoracotomy sinus rhythm

INTRODUCTION

Postoperative atrial fibrillation (poAF) is transient AF that occurs most commonly within 2-4 days after cardiac surgery in 33% of patients (1) despite beta blocker prophylaxis (2, 3). While transient, poAF increases the risk of stroke and mortality by 50% (4) and recurrent AF by eight-fold, indicating that current therapies do not adequately treat the post-surgical inflammatory changes that may lead to long-lasting sequelae (5). The degree of post-surgical inflammation directly correlates with poAF risk (6, 7), and we previously demonstrated greater NLRP3 inflammasome activity in the atria of poAF compared to sinus rhythm patients (8).

Interleukin (IL)-6 is a key inflammatory cytokine downstream of the NLRP3 inflammasome that was also elevated in the sera (9) and atria (7) of poAF patients, although these studies were focused on samples collected at the time of surgery and thus reflect the contribution of pre-existing substrate rather than post-surgical inflammation. We and others have shown IL-6 to be elevated in poAF animal models at the time of arrhythmia on postoperative day three (10-13). However, less is known about the key cell type(s) involved in IL-6 signaling or how it mechanistically promotes atrial arrhythmogenesis. Biologically, IL-6 activates the JAK/STAT3 cascade upon binding to transmembrane subunit glycoprotein 130 (gp130) and the IL-6 receptor alpha (IL-6Rα), which is expressed by hepatocytes and leukocytes, predominantly of the myeloid lineage (14). Therefore, IL-6 signaling in most cell types (i.e., atrial cardiomyocytes [ACMs]) requires the presence of nearby leukocytes to generate IL-6Rα (15) through ADAM 10 and 17-mediated ectodomain cleavage in a process known as trans-signaling (16).

Here, we demonstrate that infiltrating atrial macrophages are critical for IL-6 signaling in poAF through IL-6Rα shedding. We validated our findings in pericardial fluid samples collected from human patients after open-heart surgery as a surrogate of local cardiac inflammation, which addresses the fundamental limitation of prior studies relying on atrial samples harvested at the time of surgery. Downstream of IL-6Rα, STAT3 inhibition with FDA-orphan drug designated phosphorylated-STAT3

inhibitor TTI-101 was sufficient to prevent poAF in mice, and enhanced STAT3-CaMKII signaling led to triggered activity through CaMKII-mediated RyR2-S2814 phosphorylation and arrhythmogenic sarcoplasmic reticulum (SR) Ca^{2+} leak.

RESULTS

Macrophages are necessary for poAF. To induce poAF, a thoracotomy protocol previously described in detail (10) was performed while a sham surgery served as a control (see supplementary methods, **Figure S1A**). All mice subsequently underwent programmed electrical stimulation using intracardiac catheter burst pacing on postoperative day three to identify mice with poAF after thoracotomy (i.e., thoracotomy AF [TAF]) (10). Representative surface and atrial electrograms showing sinus rhythm and poAF in sham and thoracotomy mice, respectively are shown in **Figure S1B**, with the full poAF episode shown in **Figure S1C**. To assess the cell types involved in poAF pathogenesis, unbiased scRNAseq was performed comparing atrial non-myocytes isolated from sham and TAF mice. UMAP clustering and annotation of cell types with commonly used markers (17-19) (**Figure S2A-B**) revealed a 2.4-fold increase (P<0.001) in macrophages in the atria of TAF versus sham mice (**Figure 1A-C**). Immunohistochemical staining of mouse heart sections harvested on postoperative day three confirmed the presence of macrophages within the atria that was consistently increased in both the right and left atria of TAF versus sham mice (**Figure S3A-D**) with unaltered ventricular macrophage accumulation (**Figure S3E**). Consistent with the lack of ventricular macrophage infiltration, ventricular tachycardia (VT) inducibility was unchanged three days after thoracotomy (**Figure S4A**). Ventricular IL-6 mRNA and protein levels were increased in TAF versus sham mice, reflective of greater systemic inflammation after cardiac surgery, while ventricular IL-6Rα mRNA and protein levels were unaltered in TAF versus sham mice, consistent with the lack of ventricular macrophage accumulation given the selective expression of IL-6Rα in leukocytes (**Figure S4B-D**) (14). There was no evidence of an adaptive immune response (i.e., unchanged B and T-cell numbers) (**Figure 1B**) or histologic atrial fibrosis in the left or right atria (**Figure S5**). Thus, macrophage-mediated inflammation, not fibrosis, likely drives atrial arrhythmogenesis in our murine poAF model.

To further assess the differential contributions of macrophages to poAF pathogenesis, macrophages from our scRNAseq dataset were re-clustered, which separated them into anti-inflammatory, pro-inflammatory/infiltrating, mixed (pro/anti-inflammatory), proliferating antigen-presenting cells, and dendritic cells using cell type-specific markers (**Figure 1D, S2C**) (18). Strikingly, TAF mice exhibited a 1.5-fold (P=0.014) increase in pro-inflammatory and mixed macrophages (**Figure 1E**). To investigate possible chemoattractants driving this post-surgical increase in atrial macrophages, we assessed differential cell-cell crosstalk using CellChat, which models ligand-receptor interactions derived from scRNAseq data (20). We found a 2.5-fold increase in cell-cell communication pathways in TAF versus sham mice (**Figure S6A-B**) that was predominantly driven by an increase in macrophage-mediated signaling (**Figure S6C**). A detailed analysis of the altered signaling pathways in macrophages revealed the CCL pathway mediated by CCR2 to be a top differentially upregulated pathway in the atria of TAF versus sham mice (**Figure S6D-E**). Indeed, flow cytometry confirmed a significant increase in infiltrating $CCR2^{+}$ monocyte-derived macrophages in the atria of TAF versus sham mice (**Figure S6F-G**). Thus, our data show that chemokine signaling mediated by CCR2 drives the post-surgical infiltration of monocyte-derived macrophages into the atria.

Given the relevance of macrophages in poAF development, we sought to assess whether macrophages are necessary for poAF. To do this, macrophages were depleted in mice by intraperitoneal clodronate liposome (CL) injection one hour prior to cardiothoracic surgery (**Figure S7A**), which reduced macrophage counts by 92% in the spleen (P<0.001) three days after injection (**Figure S7B**), consistent with prior studies (21). A similar reduction (86% decrease, P<0.001) in atrial $CD11b^{+}$ macrophages was seen using flow cytometry on postoperative day three (**Figure 1F-G**). Strikingly, there was a 3.7-fold (P=0.025) reduction in poAF inducibility (**Figure 1H-I**) in macrophage-depleted versus placebo-treated mice after thoracotomy, with a concomitant trend towards decreased poAF duration (**Figure 1J**). The average AF frequency in WT mice after thoracotomy was 11.5 Hz, or 682 beats per minute, which is characteristic of the rapid ventricular response often seen in the human condition. There were no changes in electrocardiogram (ECG) parameters including RR, PR, and QRS

intervals as well as sinus node recovery time (SNRT) and atrioventricular effective refractory period (AVERP) among groups that might affect poAF inducibility through enhanced sinus node activity and/or reentry-promoting substrate alterations (**Table 1, Figure S8A**). Thus, monocyte-derived atrial macrophages are fundamentally required for poAF development.

Macrophages promote poAF through IL-6 signaling. Given that the prominent macrophage subtype in TAF mice was a mixed pro/anti-inflammatory class likely in a transitioning state, we conducted unbiased Monocle 3 pseudotime analyses (**Figure 2A**), which mathematically models dynamic changes in cell state by calculating cellular trajectories (22), to assess for key driver genes in this macrophage cell state transition. Strikingly, *Il6* was the most correlated cytokine in pseudotime, exhibiting greater spatial correlation than *Il-1β* and *Nlrp3* (**Figure 2B**), which we previously demonstrated to play a role in poAF (8). Importantly, IL-6 signaling counterparts *Socs3*, *Adam10*, and *Il6ra* were also among the top genes driving the macrophage cell state transition (**Figure 2B-D)**. Parallel cell-cell communication analyses comparing differential cell-cell interactions in sham versus TAF mice revealed that IL-6 was indeed a top differentially upregulated signaling pathway in TAF versus sham mice (**Figure 2E**). Upon further analysis of the IL-6 pathway, we found that macrophages were the most prominent drivers of IL-6 signaling (**Figure 2F**), likely through expression of *Il6ra* (**Figure 2G-H**). Thus, IL-6 signaling driven by atrial macrophages is central to poAF.

IL-6 signaling is increased in poAF.

To assess the translatability of our findings to the human condition, we collected pericardial fluid from patients after open-heart surgery as a surrogate measure of local cardiac inflammatory activity (as cardiac biopsy is not possible during the postoperative period). We first assessed whether macrophages infiltrated human hearts after cardiac surgery by collecting paired pericardial fluid samples from the same patients on postoperative days 1 and 3. Strikingly, CD68 protein levels,

indicative of macrophages, were 2.1-fold (*P*=0.005) greater on postoperative day 3 versus 1, indicating that macrophages do indeed infiltrate human hearts after cardiac surgery (**Figure 3A**). We then focused on pericardial fluid collected on postoperative day three, which is the time of peak poAF occurrence, and found that patients with poAF had 3.6-fold (*P*=0.022) and 2.9-fold (*P*=0.015) greater CD68 and IL-6 protein, respectively, compared to patients in sinus rhythm (**Figure 3B**). Apart from rhythm status, there were no differences in clinical characteristics between poAF and sinus rhythm patients (**Table S4**).

Given our findings implicating altered macrophage-mediated IL-6 in human poAF, we assessed for changes in IL-6 and its signaling counterparts in our poAF mouse model (10). After programmed electrical stimulation (PES) on postoperative day three, mice were divided into sham (Sh), mice that underwent surgery but remained in sinus rhythm (thoracotomy sinus rhythm [TSR]), and mice with poAF (thoracotomy atrial fibrillation [TAF]). Plasma IL-6 and atrial *Il6* and *Il6ra* were greatest in TAF compared to TSR and sham mice (**Figure 3C-E**). Consistent with a systemic inflammatory IL-6 response, ventricular IL-6 was increased at the mRNA and protein levels while ventricular IL-6Rα remained unchanged, reflecting the lack of ventricular macrophage infiltration (**Figure S3D-F**). Atrial IL-6 was significantly greater in TAF compared to TSR (2.0-fold, *P*=0.041) and sham (2.29-fold, *P*=0.026) mice (**Figure 3F**). Atrial gp130 protein levels were also increased in TAF versus TSR (2.2-fold, *P*=0.002) and sham (3.7-fold, *P*<0.001) mice. Interestingly, there were no differences in IL-6Rα between TAF and TSR (**Figure 3G**), in contrast to what was observed at the *Il6ra* mRNA level (**Figure 3E**). As IL-6Rα protein levels by western blot are indicative of membrane-bound IL-6Rα, these results suggest an increase in shedding of membrane-bound IL-6Rα and greater pro-inflammatory IL-6 trans-signaling. Indeed, atrial ADAM17 and ADAM10, the primary IL-6Rα sheddases (23), were greatest in TAF compared to TSR and sham mice at both the mRNA and protein levels (**Figure S9**). Taken together, IL-6 and mediators of IL-6 trans-signaling were greatest in TAF compared to sham and TSR mice. Even among age- and sex-matched mice that underwent the same cardiac surgery, only those

with poAF (TAF) exhibited increased atrial IL-6, indicating that the post-surgical increase in atrial IL-6 is likely a direct cause of poAF rather than nonspecific consequence of post-surgical inflammation.

To assess the potential relevance of a pre-existing IL-6-promoting substrate in poAF development, biochemical studies were conducted from right atrial appendages harvested at the time of cardiac surgery from patients who remained in sinus rhythm and those who developed poAF. The incidence of poAF, defined by a documented AF episode lasting ≥30 sec (24), was monitored for up to 5-days post-surgery. Clinical and demographic characteristics of patients who developed poAF versus sinus rhythm controls were similar (**Tables S5-S7**), with the exception of an association between older age and poAF status. There was a nominal increase of *IL6* mRNA and significant increase in IL-6 protein in the atria of poAF versus sinus rhythm patients at the time of surgery (**Figure S10A-B**). Due to the association between older age and poAF, we performed linear regression between age and IL-6 protein levels and found a nominally positive association (R^2=0.157, *P*=0.084; **Figure S10C**), indicating that the greater IL-6 protein levels at the time of surgery in poAF versus sinus rhythm patients is, in part, attributable to the older age of poAF versus SR patients. In contrast, IL-6 protein levels in pericardial fluid collected at the time of arrhythmia exhibited a much greater magnitude of increase in poAF versus sinus rhythm patients (**Figure 3B**), indicating that post-surgical changes in IL-6 are more pathologically important than pre-existing alterations. Like IL-6, the gp130 transmembrane subunit of the IL-6/IL-6Rα complex was elevated in the atria of poAF compared to sinus rhythm patients (**Figure S10G-H**), although there was a trend between older age and atrial gp130 levels (R^2=0.130, *P*=0.142; **Figure S10I**). Importantly, IL-6Rα was unchanged in human atrial biopsies at the time of surgery (**Figure S10D-E**) without an age correlation (R^2=0.050, *P*=0.344; **Figure S10F**), indicating that the observed increases in atrial IL-6Rα mRNA and protein measured on postoperative day three in mice (**Figure 3E,G**) occur after surgery. Taken together, differences in pre-existing atrial IL-6 are minimal compared to those that occur after surgery. In particular, the significant change in IL-6Rα after surgery

compared to that existing prior to cardiac surgery validates the observed changes in atrial immune cell profile given the selective expression of IL-6Rα in macrophages (**Figure 2G-H**).

Loss of IL-6Rα from macrophages is sufficient to rescue poAF. To further explore these findings, *Il6ra* was conditionally knocked out in macrophages by crossing *Il6ra*$^{fl/fl}$ and LysM-Cre mice (**Figure 4A**). Decreased IL-6Rα expression in F4/80^{+} splenic macrophages was validated by flow cytometry (**Figure 4B-C**). We chose to express under the LysM promoter, which hits ~70% of neutrophils,(25) given that we observed neutrophils (PMNs), in addition to macrophages, to express *Il6ra* in the atria (**Figure 2G**). Thoracotomy followed by PES studies revealed a 71% (P=0.034) reduction in poAF inducibility (**Figure 4D**), along with a 4.3-fold (P=0.018) and 3.0-fold (P<0.001) reduction in atrial IL-6Rα mRNA and protein, respectively, in *Il6ra*-cKO versus WT mice after thoracotomy (**Figure 4E-F**). Importantly, atrial Il-6 and IL-6 pathway activation by STAT3-Y705 phosphorylation were significantly attenuated in *Il6ra* cKO versus WT mice after thoracotomy (**Figure 4G-I**), demonstrating that IL-6Rα from macrophages is crucial for atrial IL-6 trans-signaling during the perioperative period. There were no differences in baseline ECG parameters, SNRT, or AVERP among groups (**Table 1, Figure S8B**). These results demonstrate that targeting the IL-6 signaling axis, specifically IL-6Rα produced by macrophages, is sufficient to rescue poAF.

STAT3-CaMKII signaling is increased in poAF. To assess the downstream consequences of enhanced IL-6 signaling in poAF, western blotting was performed on atrial tissue harvested from mice on postoperative day three. Consistent with enhanced IL-6 signaling, a significant induction of STAT3 activation by STAT3-Y705 phosphorylation was noted in the atria of TAF compared to TSR and sham mice (**Figure 5A**). As we and others have previously shown that CaMKII-mediated RyR2 phosphorylation at Ser2814 is upregulated in poAF patients (8, 11), we hypothesized that STAT3 downstream of IL-6 acts as a transcriptional activator of CaMKIIδ within cardiomyocytes, a biological

pathway that was previously reported in endothelial cells (26). Consistent with this hypothesis, we found significantly greater CaMKIIδ protein and CaMKII-mediated RyR2-Ser(S)2814 phosphorylation (27) in the atria of TAF versus TSR and sham mice (**Figure 5B-C**), suggesting that STAT3 activation downstream of IL-6 directly promotes pro-arrhythmogenic alterations in the atria.

To assess the importance of STAT3 in poAF, we pharmacologically inhibited STAT3 using S3I-201 and TTI-101, which is an FDA-orphan drug designated inhibitor of phosphorylated STAT3 (28, 29). We administered TTI-101 or S3I-201 one hour prior to surgery and then once a day for three days until the assessment of poAF inducibility on postoperative day three (**Figure 5D**). Both STAT3 inhibitors effectively blunted STAT3-Y705 phosphorylation within the atria of mice after thoracotomy on postoperative day three (**Figure S11A-B**). STAT3 inhibition with S3I-201 decreased poAF inducibility by 3.5-fold (*P*=0.043), whereas a robust 6.0-fold (*P*=0.022) reduction in poAF incidence was observed after TTI-101 treatment (**Figure 5E**) without significant changes in poAF duration (**Figure 5F**). There were no changes in baseline ECG parameters, SNRT, or AVERP among groups (**Table 1**) that might affect these results.

To directly demonstrate that STAT3 activation within cardiomyocytes plays a pro-arrhythmogenic and fundamental role in poAF development, we generated cardiomyocyte-specific *Stat3* cKO mice by expressing Cre under the *Tnt* promoter via AAV9 in *Stat3*$^{FL/FL}$ mice (**Figure 5G**). Effective *Stat3* knockdown was validated by western blot showing a 1.9-fold (*P*=0.017) decrease in atrial STAT3 (**Figure S11C**). Strikingly, phospho-Y705 (i.e., activated) STAT3 exhibited a stronger decrease than total STAT3, suggesting that the major pool of activated STAT3 after thoracotomy lies within ACMs. Indeed, these *Stat3* cKO mice were protected from poAF incidence (5.4-fold reduction, *P*=0.029; **Figure 5H**) and duration (2.6-fold decrease, *P*=0.062; **Figure 5I**). No significant differences were observed in baseline ECG parameters (**Table S8**) or inducibility of ventricular arrhythmias (data not shown). Taken together, IL-6 upregulates CaMKIIδ in a STAT3-dependent manner in cardiomyocytes, leading to RyR2-S2814 phosphorylation and triggered activity.

IL-6 promotes arrhythmogenic RyR2-mediated SR Ca^{2+} leak.

To definitively show that ectopic (triggered) activity, not reentry, was the predominant driver of atrial arrhythmogenesis in poAF, we conducted optical mapping on ex-vivo Langendorff-perfused mouse hearts. Conduction velocity and coefficient of variation measured at 10 Hz pacing did not significantly differ in thoracotomy versus sham mice in the right (**Figure 6A-C**) or left (**Figure 6D-F**) atria, consistent with a lack of reentrant-prone substrate alterations. In contrast, we observed a significant increase in triggered activity without evidence of reentry (i.e., rotors) originating from ectopic foci within the atria distant from the pacing site, following S1-S2 pacing (**Figure 6G-H**). Consistent with triggered activity as the key driver of atrial arrhythmogenesis in poAF, *ex-vivo* hearts from mice after thoracotomy had a significantly greater incidence of atrial tachyarrhythmias (**Figure 6I**) and triggered activity (**Figure 6J**) without changes in atrial refractoriness (**Figure 6K**).

Next, to assess the molecular mechanisms by which IL-6 leads to triggered activity, we challenged of primary wild-type mouse cardiomyocytes with IL-6 + IL-6Rα (IL-6/R), which increased *Camk2d* mRNA by 1.71-fold (P=0.027) after 30-minutes (**Figure 7A**) and CaMKIIδ protein by 1.99-fold (P=0.039) after 2-h (**Figure 7B-D**), respectively, consistent with the hypothesized transcriptional upregulation of CaMKIIδ by STAT3**.** To determine whether this STAT3-mediated CaMKII upregulation was pro-arrhythmogenic, we performed Ca^{2+} imaging in ACMs isolated from wild-type (WT) mice that were treated with vehicle or IL-6/R for 1.5-h. ACMs were conditioned by pacing at 1-Hz followed by a 60-second pause during which Ca^{2+} sparks and Ca^{2+} waves, defined as >25% of the Ca^{2+} transient amplitude, were measured. The protocol was finished by assessing SR Ca^{2+} load via acute 10 mM caffeine exposure (**Figure 7E-F**). The amplitude of systolic paced Ca^{2+} transients trended lower after IL-6/R treatment (P=0.270, **Figure 7G**), suggestive of enhanced diastolic Ca^{2+} leak and consistent with prior studies (30). Importantly, there was a 3.2-fold (P=0.046) increase in diastolic Ca^{2+} spark frequency in IL-6/R versus vehicle-treated ACMs (**Figure 7H**). As SR Ca^{2+} load was unaffected by IL-6/R treatment (P=0.924, **Figure 7I**), the increase in Ca^{2+} spark frequency remained significant after

normalization by SR Ca^{2+} load (*P*=0.024, **Figure 7J**). Indeed, the incidence (2.5-fold, *P*=0.011; **Figure 7K**) and duration (2.9-fold, *P*=0.031; **Figure S12A**) of spontaneous Ca^{2+} waves, which are strongly correlated with greater arrhythmogenic potential (31), were greater in IL-6/R versus vehicle-treated ACMs despite no differences in wave latency (**Figure S12B**). Altogether, these results indicate that CaMKII-mediated RyR2 dysfunction was the primary arrhythmogenic driver downstream of IL-6.

CaMKII inhibition rescues arrhythmogenic SR Ca^{2+} leak.

To assess whether enhanced CaMKII signaling was responsible for the observed changes in ACM Ca^{2+} handling, ACMs were isolated from sham and TAF mice, and confocal imaging of Ca^{2+} handling was performed. Paced Ca^{2+} transient amplitude did not differ among groups (**Figure S13A-B**), although there was a trend towards decreased transient amplitude after KN-93 treatment as expected with CaMKII inhibition (*P*=0.677, **Figure S13B**). No differences in Ca^{2+} transient decay were observed among groups, suggesting that alterations in SERCA2a-mediated Ca^{2+} reuptake likely play a minor role in poAF (**Figure S13C**). We then assessed arrhythmogenic diastolic Ca^{2+} sparks after 1-Hz field pacing (**Figure 8A**). ACMs from TAF mice exhibited 1.9-fold (*P*=0.002) and 6.6-fold (*P*<0.001) greater Ca^{2+} spark frequency compared to ACMs from TSR and Sh mice, respectively (**Figure 8B**). Importantly, KN-93 pre-treatment of TAF ACMs was sufficient to reverse these changes (3.5-fold decrease, *P*<0.001), indicating that CaMKII is necessary for arrhythmogenic Ca^{2+} sparks in poAF (**Figure 8B**). As SR Ca^{2+} load was unchanged among groups (**Figure 8C**), similar trends held for Ca^{2+} spark frequency after normalization to SR Ca^{2+} load (**Figure 8D**), implicating RyR2 Ca^{2+} leak as the primary pro-arrhythmogenic mechanism in poAF. Indeed, the incidence (**Figure 8E**) and duration (**Figure S12C**) of spontaneous Ca^{2+} waves were greatest in ACMs from TAF compared Sh and TSR mice. Interestingly, wave latency was similarly decreased in ACMs from TSR and TAF mice compared to Sh, suggesting that faster wave onset may be a nonspecific consequence of cardiac surgery rather than a direct cause of poAF (**Figure S12D**). These findings were unaffected when by KN-93 inactive analogue, KN-92, different doses (1 μM vs 2.5 μM) of KN-93 (**Figure S14A-B**), or pacing at 2 Hz versus 1 Hz (**Figure**

S15A-B). Thus, arrhythmogenic RyR2 Ca^{2+} sparks and waves are direct associated with poAF development as they were absent in ACMs from TSR and Sh mice, and CaMKII inhibition was sufficient to revert this pro-arrhythmogenic Ca^{2+} mishandling phenotype.

Lastly, to definitively show that RyR2-S2814 phosphorylation by CaMKII and subsequent Ca^{2+} mishandling is necessary for poAF, we performed cardiac surgeries in non-phosphorylatable *RyR2*^{S2814A} mice and phosphomimetic *RyR2*^{S2814D} mice. Baseline ECG parameters including SNRT and AVERP did not differ among groups, although there was a trend towards faster heart rate in RyR2 phosphomutant mice (**Table 1, Figure S8C-D**). Strikingly, nonphosphorylatable *RyR2*^{S2814A} mice were protected from poAF compared to WT littermates (80% decrease, P=0.047; **Figure 8F-G**) independent of atrial IL-6 protein levels (**Figure S16A-B**), demonstrating that RyR2-S2814 phosphorylation is downstream of IL-6. While *RyR2*^{S2814D} mice did not exhibit greater poAF inducibility, likely a result of RyR2-S2814 phosphorylation levels already exerting a near-maximal pro-arrhythmogenic effect after cardiac surgery, these phosphomimetic *RyR2*^{S2814D} mice exhibited a trend towards longer poAF duration (mean poAF duration 200s in *RyR2*^{S2814D} vs 66s in WT; **Figure 8H**). Taken together, the phosphorylation of RyR2-S2814 by CaMKII, as opposed to CaMKII effects on other ion channels such as the late sodium current (32, 33), is a necessary action of CaMKII in poAF development.

DISCUSSION

Our study is the first, to our knowledge, to assess the single-cell transcriptomic landscape of poAF in a clinically relevant mouse model using scRNAseq. Moreover, our studies in pericardial fluid collected from human patients after open-heart surgery address a fundamental knowledge gap in the current understanding of poAF as prior studies have relied on human atrial tissue collected at the time of surgery (8, 34-37) and thus reflect pre-existing substrate rather than the contribution of surgical-induced inflammation, which is more amenable to therapeutic intervention given its acute and transient nature. Our translational findings center around observations after cardiac surgery in human patients and mice and show that infiltrating atrial macrophages are fundamentally required for poAF development through generation of the IL-6 receptor. Downstream of IL-6, STAT3 inhibition with FDA-orphan drug TTI-101 and cardiomyocyte-specific *Stat3* cKO prevented poAF, indicating that activated STAT3 specifically within ACMs plays a direct pro-arrhythmogenic in poAF. At the single ACM level, IL-6/R directly induced arrhythmogenic Ca^{2+} mishandling through RyR2 dysfunction in a CaMKII-dependent manner, leading to triggered activity and poAF. Thus, our data suggest that targeting of the IL-6 receptor and downstream signaling in atrial macrophages may represent a novel therapeutic approach for the prevention of poAF.

Macrophages infiltrating the atria play a central role in poAF

Our results implicate, in an unbiased manner, infiltrating monocyte-derived macrophages as a central cell type contributing to poAF (**Figures 1A-B, S6F-G**). We have previously demonstrated increased macrophages in the atria of patients with versus without poAF, although these samples were importantly taken at the time of surgery (8) and thus do not reflect the contribution of surgery-mediated inflammation. We have built upon this prior finding using pericardial fluid collected after cardiac surgery to show that a greater quantity of macrophages infiltrates the heart after cardiac surgery in patients with versus without poAF (**Figure 3A-B**). Our novel findings in the perioperative period of cardiac surgery

patients confirm that the results we and others (11, 38) have shown regarding the importance of macrophages in small animal poAF models translates to the human condition.

Furthermore, we build upon the prior literature by demonstrating that macrophage depletion is sufficient to prevent poAF (**Figure 1H**). We identified CCR2 as a likely upstream chemoattractant receptor driving atrial macrophage infiltration (**Figure S6D-G**). Indeed, MCP-1, the ligand for CCR2, was increased in the pericardial effluent of patients 48-h after cardiac surgery (39). Consistent with the role of MCP-1 in macrophage recruitment, we found that macrophages infiltrated human hearts after cardiac surgery to a greater extent in poAF versus SR patients (**Figure 3A-B**). Downstream of atrial macrophage infiltration, we utilized pseudotime trajectory analyses to identify *Il-6* as a central regulatory gene of macrophage cell state (**Figure 2B**), which we confirmed to be upregulated in poAF patients (**Figure 3B**). Indeed, CellChat revealed that macrophages were the predominant cell type driving upregulated IL-6 signaling in poAF (**Figure 2F**). Moreover, by comparing human atrial tissue collected at the time of surgery to mouse atria collected at the time of arrhythmia, we found that IL-6Rα was the only protein in the IL-6 signaling cascade that progressed from unchanged at the time of surgery (**Figure S10E**) to increase at the time of arrhythmia (**Figure 3G**), suggesting that IL-6Rα may be amenable to therapeutic intervention.

IL-6 receptor signaling in macrophages is essential for poAF development

To test whether IL-6 receptor signaling in macrophages is essential for poAF development, we generated macrophage-specific *Il6ra* conditional knockout mice. These *Il6ra*-cKO mice were protected against the development of inducible poAF after thoracotomy (**Figure 4G**). Indeed, mice that underwent thoracotomy did not exhibit greater ventricular tachycardia inducibility compared to sham, consistent with the lack of macrophage-dependent IL-6Rα production and subsequent IL-6 trans-signaling (**Figure S4**). Prior studies focused on the ligand (IL-6) and demonstrated that global *Il-6* knockout (13) and IL-6 pharmacologic inhibition (11) protected against poAF in rat sterile pericarditis models (**Table S9**).

However, these studies, in particular global *Il6* knockout, are confounded by indirect pro-arrhythmogenic alterations such as metabolic dysfunction (14, 40). Moreover, nonspecific inhibition of IL-6 blunts classical IL-6 signaling, which is anti-inflammatory, and thus may aggravate the pro-inflammatory post-surgical response, making this approach clinically undesirable (41). Indeed, a recent preclinical study of chronic AF in mice demonstrated that selective neutralization of IL-6 trans-signaling via soluble gp130 ameliorated AF inducibility induced by chronic pressure overload (42). However, this paper focused on the role of IL-6 signaling in chronic atrial substrate alterations through connexin and fibrotic remodeling, which our data did not reveal to change in our 72-hour poAF mouse model (**Figure S5; Table S9**).

IL-6 receptor signaling involves the STAT3 pathway, which was elevated in TAF mice compared to those that underwent cardiac surgery but remained in sinus rhythm (i.e., TSR; **Figure 5A**). We then performed in vivo studies to test the hypothesis that STAT3 inhibition could prevent poAF in our mouse model. Indeed, our studies revealed that STAT3 inhibition with TTI-101, an inhibitor of phosphorylated STAT3 (28), prevented poAF in mice (**Figure 5E**). These findings suggest that drug repurposing might be a future option for TTI-101, which is currently in phase 2 clinical trials for hepatocellular carcinoma (NCT05440708), metastatic breast cancer (NCT05384119), and idiopathic pulmonary fibrosis (NCT05671835).

IL-6 receptor-dependent arrhythmogenic mechanisms in poAF

STAT3 is a transcription factor, widely known for its role in fibrosis in the heart (12). Nonetheless, consistent with prior findings in poAF patients (8) and animal models (11), we did not find evidence of a change in fibroblast proliferation (**Figure 1A-B**) nor evidence of histologic fibrosis (**Figure S5**) in our poAF mouse model. Regardless, the use of antifibrotic therapies in patients during the perioperative period would likely be contraindicated due to impaired wound healing and risk of infection (43, 44). Taken together with the lack of changes in atrial conduction velocity in mice after thoracotomy versus sham surgery (**Figure 6A-F**), our data show that reentry is unlikely the primary arrhythmogenic

mechanism in poAF, although our optical mapping studies were limited by two-dimensional recordings and we did not pace at supraphysiologic frequencies, which may have been necessary to uncover heterogenous conduction. Nonetheless, our data point towards triggered activity as the primary driver of atrial arrhythmogenesis in poAF (**Figure 6G-J**). Molecularly, we found that IL-6-mediated STAT3 activation plays a direct pro-arrhythmogenic role in cardiomyocytes through CaMKIIδ upregulation (**Figure 7A-D**) as cardiomyocyte-specific *Stat3* cKO prevented poAF in mice (**Figure 5H**). CaMKIIδ is the predominant CaMKII isoform in the heart(45) that is activated during the normal cardiac stress response (46, 47). When overactive, however, CaMKII can cause arrhythmia, particularly AF (48, 49) through RyR2-S2814 hyperphosphorylation (27) and resultant arrhythmogenic Ca^{2+} sparks (50, 51). Importantly, Ruxolitinib, originally discovered as a JAK inhibitor upstream of STAT3, was recently shown to possess CaMKII inhibitory properties and protect against ventricular arrhythmias (52). Our findings implicate enhanced STAT3-CaMKII signaling in poAF development (**Figure 5A-C**), thus providing evidence that Ruxolitinib may be a potential candidate for drug repurposing for poAF.

Functionally, we found that IL-6 (or IL-6 receptor activation) recapitulates the Ca^{2+} mishandling observed in poAF as IL-6/R treatment alone was sufficient to increase SR load-normalized Ca^{2+} sparks and Ca^{2+} waves in isolated ACMs (**Figure 7J**), pointing to RyR2 dysfunction as the likely arrhythmogenic driver. However, it is important to consider the role of other known drivers of sarcoplasmic reticulum Ca^{2+} mishandling such as stress kinase JNK2 (c-Jun N-terminal kinase isoform 2), which is currently being explored a novel gene therapy for primary AF (53). Our results are consistent with prior studies demonstrating cardiac Ca^{2+} mishandling in poAF patients (8, 54) and rats (11), although these studies were conducted at the time of arrhythmia or at the whole heart level, respectively, and thus may not completely delineate the molecular Ca^{2+} mishandling phenotype present at the time of arrhythmia at the single ACM level as we have done in our study (**Table S9**). We further demonstrate that ACMs from TAF mice exhibited significantly greater arrhythmogenic Ca^{2+} sparks and waves compared to those from TSR and that CaMKII inhibition was sufficient these ameliorate these

arrhythmogenic changes (**Figure 8B-E**). Lastly, to definitely show that the actions of CaMKII on RyR2-S2814 phosphorylation were central to poAF pathophysiology as opposed to CaMKII effects on other ion channels such as the late sodium current (32, 33), we demonstrated that non-phosphorylatable *RyR2*^{S2814A} mice were protected from poAF (**Figure 8F**). Taken together, our data show that aberrant SR Ca^{2+} release via RyR2-S2814 hyperphosphorylated channels promotes the development of cellular triggered activity in poAF and that these arrhythmogenic events are downstream of IL-6-mediated STAT3 activation in ACMs.

Potential Limitations

Our study has several limitations. Our studies of human atrial tissue from patients with poAF were cross-sectional in nature. Therefore, longitudinal associations between baseline atrial biochemical measurements and incident clinical sequalae could not be derived. We observed a marked induction of *Il6ra* expression in neutrophils, in addition to macrophages. Although the LysM-Cre transgenic mouse we used reportedly expresses in up to 70% of neutrophils (25), we cannot exclude that the remaining neutrophil-expressed IL-6Rα had subclinical effects on atrial arrhythmogenesis, although we detected a robust reduction in total atrial IL-6Rα mRNA and protein in *Il6ra* cKO mice (**Figure 4E-F**) and macrophage-specific *Il6ra* cKO attenuated IL-6 downstream STAT3 activation (**Figure 4H-I**). In addition, it is possible that neutrophils activate the IL-6 pathway through indirect effects such as IL-1β-mediated IL-6 activation (55) or Oncostatin-M (56). Future studies would benefit from utilizing neutrophil-specific Cre lines such as Ly6G-Cre to dissect the differential contributions of neutrophils versus macrophages in poAF pathogenesis (25). Indeed, neutrophil-derived myeloperoxidase, in part promoted by reactive oxygen species (57) was shown to promote AF through atrial fibrotic remodeling (58). Moreover, CaMKII activation via oxidation is a well-known driver of AF (59, 60), and we found CaMKII-mediated RyR2-S2814 phosphorylation to play a fundamental role in atrial arrhythmogenesis

in our murine poAF model. It is also critical to note that CaMKII phosphorylation of other ion channels, in particular sodium channels (61, 62), could play a key role in poAF initiation and maintenance. In addition, another limitation of our studies is the use of sub-physiologic pacing frequencies (i.e., 1-2 Hz) in our confocal Ca^{2+} imaging experiments of isolated ACMs. While these frequencies were sufficient to bring out significant differences in spontaneous Ca^{2+} sparks and waves in ACMs from TAF versus Sham mice (**Figure 8B-E**), it is possible that field pacing at more "physiologic" rates (i.e., 10-Hz) could have brought out even greater differences, although the rapid decay of functionality of ex-vivo ACMs limited our ability to conduct such studies. We did not directly assess inflammation-driven fibroblast activation in our poAF mice. While we did not observe differences in histologic atrial fibrosis (**Figure S5**), it is possible that activated fibroblasts may portend pro-arrhythmogenic effects independent of collagen deposition such as direct electrical coupling to cardiomyocytes or release of pro-inflammatory cytokines (63, 64). Lastly, the mice used in our study (12-15-weeks) were relatively young and disease-free, in contrast to human patients that undergo cardiac surgery and often have multiple comorbidities. Thus, poAF in our mouse model required atrial burst pacing to induce episodes of AF, like other preclinical poAF models (11, 12). However, it is important to note that our mouse studies build upon prior studies (11-13) by including the clinically relevant comparison between mice that underwent surgery and remained in sinus rhythm (TSR) versus those that developed poAF (TAF). Most animal studies of poAF (11-13) include two groups: sham versus surgery, which prevents parsing out nonspecific consequences of cardiac surgery versus direct causes of poAF. Therefore, while our mouse model may not fully recapitulate the pathophysiology of spontaneous poAF seen in patients, we believe that our results are clinically translatable to the human condition.

Conclusions

Taken together, our study demonstrates a novel paradigm of poAF whereby macrophages infiltrate damaged atria after cardiac surgery, releasing soluble IL-6Rα and driving a surge in IL-6-mediated STAT3 activation within ACMs. STAT3 upregulates CaMKIIδ, leading to phosphorylation of RyR2 at Ser2814, SR Ca^{2+} leak, and ultimately poAF. Our study has the potential to spark the design of future clinical trials and drug repurposing as we provide robust mechanistic insights on a targetable molecular pathway with current FDA-approved therapies such as IL-6Rα monoclonal antibodies (Tocilizumab), CaMKII inhibitors (Ruxolitinib), and RyR2 antagonists (flecainide) or investigational drugs such as STAT-3 inhibitor TTI-101, that may be used for poAF prevention and treatment.

METHODS

Sex as a biological variable. For all human and murine studies, equal numbers of male and female subjects were used when possible. For mice, controls consisted of wild-type littermates when possible.

Mouse procedures. Our mouse model of poAF was designed to recapitulate cardiac surgery as described in detail (see Supplementary Materials) (10). In vivo electrophysiology studies for poAF assessment were performed as previously described (see Supplementary Materials) (10, 65).

Single-cell RNA sequencing (scRNAseq) comparing atrial non-myocytes from sham and TAF mice was performed as described in detail in the Supplementary Materials .

Flow cytometry was conducted as described in detail in the Supplementary Materials using the antibodies list in **Table S1**.

Mouse Plasma Collection. Mouse blood was collected by cardiac puncture with 25G needle/syringe coated with heparin (McKesson Corporation, Memphis, TN). Whole blood was allowed to equilibrate at room temperature for 30 minutes prior to spinning at 2000 x g for 15 minutes at 4°C. The supernatant (plasma) was removed and stored at -80°C.

Real-Time Quantitative Polymerase Chain Reaction (RT-qPCR). Total RNA was isolated from atrial tissues by TRIzol (15596, Life technologies, Carlsbad, CA), and 500 µg of RNA was reverse transcribed by iScript (1708841, Bio-Rad, Hercules, CA). The iTaq Universal SYBR Green Supermix (Thermo Fisher Scientific, Waltham, MA) with 1 µM primer and diluted cDNA 1:25 was used for the quantitative

polymerase chain reaction (PCR). Thermocycler conditions were 40 cycles of denaturation at 95°C for 15s and annealing and extension step of 60°C for 60s. The ΔΔCT method was used to calculate relative quantities normalized to GAPDH. Primers used are listed in **Table S2**. Digital PCR (dPCR) analyses of human right atrial appendages was performed as described in the supplementary methods.

Western Blotting. Western blotting was performed as described in detail in the Supplementary Materials using the antibodies listed in **Table S3**.

Immunohistochemistry. Immunohistochemistry was performed as described in detail in the Supplementary Materials.

Ca^{2+} imaging studies in isolated ACMs were performed as described in detail the Supplementary Materials.

Statistical Analysis. All studies and analyses were performed in a blinded manner when possible. Statistics were performed with Prism version 10.1.1 (GraphPad, La Jolla, CA). Continuous data are expressed as mean ± standard error of the mean (SEM). $P<0.05$ was considered statistically significant. The statistical test used for each figure panel described within each corresponding figure legend. Please refer to the supplemental methods for more details.

Study Approval. All animal studies were performed according to protocols approved by the Institutional Animal Care and Use Committee of Baylor College of Medicine conforming to the Guide for the Care and Use of Laboratory Animals published by the US National Institutes of Health (Publication no. 85-23, revised 1996). *Il6ra*$^{fl/fl}$, *LysM*-Cre, and *Stat3*$^{FL/FL}$ mice were acquired from Jackson Labs (Bar Harbor, ME). All mice included in this study were 12-15 week-of-age and C57BL/6J background. Collection of

human pericardial fluid was approved by the local institutional review board at the Baylor College of Medicine, Houston, Texas, United States (Protocol #H-46755). Written informed consent to participate in the study was obtained from every human subject prior to pericardial fluid collection. Collection of human right atrial appendages at the time of surgery was approved by the local ethical review board of the University Duisburg-Essen, Germany (Protocol #12-5268-BO). Written informed consent to participate in the study was obtained from each patient prior to cardiac surgery. See the Supplementary Materials for more details on subject selection criteria.

Data Availability. All data in this study are available from the corresponding author upon reasonable request. Supporting data values for each individual data point are available for download. Data from scRNAseq experiments are publicly available in the National Center for Biotechnology Information BioProject Repository (PRJNA1220606).

Author contributions

Designed research studies: J.A.K., Y.A.S., X.H.T.W.

Conducted experiments: J.A.K., Y.A.S., J.A.N.G., I.O., L.L, A.P., I.A.T., M.T., F.B., S.Z.

Acquired data: J.A.K., Y.A.S., J.A.N.G., I.O., A.P., I.A.T., M.T., F.B., M.K., M.G.C., L.L., N.L.

Analyzed data: J.A.K., Y.A.S., I.O., A.P., I.A.T., M.T., F.B., H.Y.S.

Wrote the manuscript: J.A.K., Y.A.S., H.Y.S., D.D., X.H.T.W.

Acknowledgements

The authors thank Annette Kötting-Dorsch, Dennis Hoffmann, and Simone Olesch for assistance with western blotting and digital PCR of human samples as well as Sylvia Metze and Lu Yang, PhD for technical assistance with patch clamp experiments in human atrial cardiomyocytes (all from the Institute of Pharmacology, West German Heart and Vascular Center, University Duisburg-Essen, Essen, Germany).

Financial support and sponsorship

This work was supported by National Institutes of Health grants R01-HL165704 (to D.D.), R01-HL163277, R01-HL164838, and R01-HL136389 (to N.L. and D.D.), R01-HL166832 (to M.G.C.), R01-HL147108 and R01-HL153350 (to X.H.T.W.), R01-HL160992 and R01-HL089598 (to X.H.T.W. and D.D.), 1F30-HL172431 (to J.A.K.), the European Union (large-scale integrative project MAESTRIA, No. 965286 to D.D.), Deutsche Forschungsgemeinschaft (Research Training Group No. 2989 to D.D.), American Heart Association Established Investigator Award (93611 to N.L.) the Robert and Janice McNair Foundation McNair MD/PhD Scholars Program (J.A.K.), and the Baylor College of Medicine Medical Scientist Training Program (J.A.K.).

REFERENCES

1. Dobrev D, Aguilar M, Heijman J, Guichard JB, and Nattel S. Postoperative atrial fibrillation: mechanisms, manifestations and management. *Nat Rev Cardiol.* 2019;16(7):417-36.
2. Joglar JA, Chung MK, Armbruster AL, Benjamin EJ, Chyou JY, Cronin EM, et al. 2023 ACC/AHA/ACCP/HRS Guideline for the Diagnosis and Management of Atrial Fibrillation: A Report of the American College of Cardiology/American Heart Association Joint Committee on Clinical Practice Guidelines. *Circulation.* 2024;149(1):e1-e156.
3. Norhayati MN, Shaiful Bahari I, Zaharah S, Nik Hazlina NH, Mohammad Aimanazrul Z, and Irfan M. Metoprolol for prophylaxis of postoperative atrial fibrillation in cardiac surgery patients: systematic review and meta-analysis. *BMJ Open.* 2020;10(10):e038364.
4. Lin MH, Kamel H, Singer DE, Wu YL, Lee M, and Ovbiagele B. Perioperative/Postoperative Atrial Fibrillation and Risk of Subsequent Stroke and/or Mortality. *Stroke.* 2019;50(6):1364-71.
5. Ahlsson A, Fengsrud E, Bodin L, and Englund A. Postoperative atrial fibrillation in patients undergoing aortocoronary bypass surgery carries an eightfold risk of future atrial fibrillation and a doubled cardiovascular mortality. *Eur J Cardiothorac Surg.* 2010;37(6):1353-9.
6. Ucar HI, Tok M, Atalar E, Dogan OF, Oc M, Farsak B, et al. Predictive significance of plasma levels of interleukin-6 and high-sensitivity C-reactive protein in atrial fibrillation after coronary artery bypass surgery. *Heart Surg Forum.* 2007;10(2):E131-5.
7. Kaireviciute D, Blann AD, Balakrishnan B, Lane DA, Patel JV, Uzdavinys G, et al. Characterisation and validity of inflammatory biomarkers in the prediction of post-operative atrial fibrillation in coronary artery disease patients. *Thromb Haemost.* 2010;104(1):122-7.
8. Heijman J, Muna AP, Veleva T, Molina CE, Sutanto H, Tekook M, et al. Atrial Myocyte NLRP3/CaMKII Nexus Forms a Substrate for Postoperative Atrial Fibrillation. *Circ Res.* 2020;127(8):1036-55.

9. Gaudino M, Andreotti F, Zamparelli R, Di Castelnuovo A, Nasso G, Burzotta F, et al. The -174G/C interleukin-6 polymorphism influences postoperative interleukin-6 levels and postoperative atrial fibrillation. Is atrial fibrillation an inflammatory complication? *Circulation.* 2003;108 Suppl 1:II195-9.
10. Keefe JA, Navarro-Garcia JA, Ni L, Reilly S, Dobrev D, and Wehrens XHT. In-depth characterization of a mouse model of postoperative atrial fibrillation. *J Cardiovasc Aging.* 2022;2.
11. Liao J, Zhang S, Yang S, Lu Y, Lu K, Wu Y, et al. Interleukin-6-Mediated-Ca(2+) Handling Abnormalities Contributes to Atrial Fibrillation in Sterile Pericarditis Rats. *Front Immunol.* 2021;12:758157.
12. Huang Z, Chen XJ, Qian C, Dong Q, Ding D, Wu QF, et al. Signal Transducer and Activator of Transcription 3/MicroRNA-21 Feedback Loop Contributes to Atrial Fibrillation by Promoting Atrial Fibrosis in a Rat Sterile Pericarditis Model. *Circ Arrhythm Electrophysiol.* 2016;9(7):e003396.
13. Liu Y, Wu F, Wu Y, Elliott M, Zhou W, Deng Y, et al. Mechanism of IL-6-related spontaneous atrial fibrillation after coronary artery grafting surgery: IL-6 knockout mouse study and human observation. *Transl Res.* 2021;233:16-31.
14. McFarland-Mancini MM, Funk HM, Paluch AM, Zhou M, Giridhar PV, Mercer CA, et al. Differences in wound healing in mice with deficiency of IL-6 versus IL-6 receptor. *J Immunol.* 2010;184(12):7219-28.
15. Kishimoto T. Interleukin-6: from basic science to medicine--40 years in immunology. *Annu Rev Immunol.* 2005;23:1-21.
16. Rose-John S. Interleukin-6 biology is coordinated by membrane bound and soluble receptors. *Acta Biochim Pol.* 2003;50(3):603-11.

17. Li Y, Ren P, Dawson A, Vasquez HG, Ageedi W, Zhang C, et al. Single-Cell Transcriptome Analysis Reveals Dynamic Cell Populations and Differential Gene Expression Patterns in Control and Aneurysmal Human Aortic Tissue. *Circulation.* 2020;142(14):1374-88.
18. Hulsmans M, Schloss MJ, Lee IH, Bapat A, Iwamoto Y, Vinegoni C, et al. Recruited macrophages elicit atrial fibrillation. *Science.* 2023;381(6654):231-9.
19. Bajpai G, Schneider C, Wong N, Bredemeyer A, Hulsmans M, Nahrendorf M, et al. The human heart contains distinct macrophage subsets with divergent origins and functions. *Nat Med.* 2018;24(8):1234-45.
20. Jin S, Guerrero-Juarez CF, Zhang L, Chang I, Ramos R, Kuan CH, et al. Inference and analysis of cell-cell communication using CellChat. *Nat Commun.* 2021;12(1):1088.
21. Nguyen T, Du J, and Li YC. A protocol for macrophage depletion and reconstitution in a mouse model of sepsis. *STAR Protoc.* 2021;2(4):101004.
22. Trapnell C, Cacchiarelli D, Grimsby J, Pokharel P, Li S, Morse M, et al. The dynamics and regulators of cell fate decisions are revealed by pseudotemporal ordering of single cells. *Nature Biotechnology.* 2014;32(4):381-6.
23. Garbers C, Janner N, Chalaris A, Moss ML, Floss DM, Meyer D, et al. Species specificity of ADAM10 and ADAM17 proteins in interleukin-6 (IL-6) trans-signaling and novel role of ADAM10 in inducible IL-6 receptor shedding. *J Biol Chem.* 2011;286(17):14804-11.
24. Frendl G, Sodickson AC, Chung MK, Waldo AL, Gersh BJ, Tisdale JE, et al. 2014 AATS guidelines for the prevention and management of perioperative atrial fibrillation and flutter for thoracic surgical procedures. *The Journal of thoracic and cardiovascular surgery.* 2014;148(3):e153-93.
25. Abram CL, Roberge GL, Hu Y, and Lowell CA. Comparative analysis of the efficiency and specificity of myeloid-Cre deleting strains using ROSA-EYFP reporter mice. *J Immunol Methods.* 2014;408:89-100.

26. O'Brien BJ, Singer HA, Adam AP, and Ginnan RG. CaMKIIdelta is upregulated by pro-inflammatory cytokine IL-6 in a JAK/STAT3-dependent manner to promote angiogenesis. *FASEB J.* 2021;35(4):e21437.
27. Wehrens XH, Lehnart SE, Reiken SR, and Marks AR. Ca2+/calmodulin-dependent protein kinase II phosphorylation regulates the cardiac ryanodine receptor. *Circ Res.* 2004;94(6):e61-70.
28. Xu X, Kasembeli MM, Jiang X, Tweardy BJ, and Tweardy DJ. Chemical probes that competitively and selectively inhibit Stat3 activation. *PLoS One.* 2009;4(3):e4783.
29. Hoffman KA, Villar MJ, Poveda C, Bottazzi ME, Hotez PJ, Tweardy DJ, et al. Signal Transducer and Activator of Transcription-3 Modulation of Cardiac Pathology in Chronic Chagasic Cardiomyopathy. *Front Cell Infect Microbiol.* 2021;11:708325.
30. Lin AE, Bapat AC, Xiao L, Niroula A, Ye J, Wong WJ, et al. Clonal Hematopoiesis of Indeterminate Potential With Loss of Tet2 Enhances Risk for Atrial Fibrillation Through Nlrp3 Inflammasome Activation. *Circulation.* 2024.
31. Mattiazzi A, Argenziano M, Aguilar-Sanchez Y, Mazzocchi G, and Escobar AL. Ca2+ Sparks and Ca2+ waves are the subcellular events underlying Ca2+ overload during ischemia and reperfusion in perfused intact hearts. *J Mol Cell Cardiol.* 2015;79:69-78.
32. Chin CG, Chen YC, Lin YK, Lu YY, Cheng WL, Chung CC, et al. Effect of macrophage migration inhibitory factor on pulmonary vein arrhythmogenesis through late sodium current. *Europace.* 2023;25(2):698-706.
33. Ni H, Morotti S, Zhang X, Dobrev D, and Grandi E. Integrative human atrial modelling unravels interactive protein kinase A and Ca2+/calmodulin-dependent protein kinase II signalling as key determinants of atrial arrhythmogenesis. *Cardiovasc Res.* 2023;119(13):2294-311.
34. Zaman JA, Harling L, Ashrafian H, Darzi A, Gooderham N, Athanasiou T, et al. Post-operative atrial fibrillation is associated with a pre-existing structural and electrical substrate in human right atrial myocardium. *Int J Cardiol.* 2016;220:580-8.

35. Lezoualc'h F, Steplewski K, Sartiani L, Mugelli A, Fischmeister R, and Bril A. Quantitative mRNA analysis of serotonin 5-HT4 receptor isoforms, calcium handling proteins and ion channels in human atrial fibrillation. *Biochem Biophys Res Commun.* 2007;357(1):218-24.
36. Swartz MF, Fink GW, Sarwar MF, Hicks GL, Yu Y, Hu R, et al. Elevated pre-operative serum peptides for collagen I and III synthesis result in post-surgical atrial fibrillation. *J Am Coll Cardiol.* 2012;60(18):1799-806.
37. Grammer JB, Bohm J, Dufour A, Benz M, Lange R, and Bauernschmitt R. Atrial fibrosis in heart surgery patients Decreased collagen III/I ratio in postoperative atrial fibrillation. *Basic Res Cardiol.* 2005;100(3):288-94.
38. Parent S, Vaka R, Risha Y, Ngo C, Kanda P, Nattel S, et al. Prevention of atrial fibrillation after open-chest surgery with extracellular vesicle therapy. *JCI Insight.* 2023;8(15).
39. Fatehi Hassanabad A, Schoettler FI, Kent WDT, Adams CA, Holloway DD, Ali IS, et al. Cardiac surgery elicits pericardial inflammatory responses that are distinct compared with postcardiopulmonary bypass systemic inflammation. *JTCVS Open.* 2023;16:389-400.
40. Kistner TM, Pedersen BK, and Lieberman DE. Interleukin 6 as an energy allocator in muscle tissue. *Nature Metabolism.* 2022;4(2):170-9.
41. Rose-John S. IL-6 trans-signaling via the soluble IL-6 receptor: importance for the pro-inflammatory activities of IL-6. *Int J Biol Sci.* 2012;8(9):1237-47.
42. Li X, Wu X, Chen X, Peng S, Chen S, Zhou G, et al. Selective blockade of interleukin 6 trans-signaling depresses atrial fibrillation. *Heart Rhythm.* 2023.
43. Seo C, Michie C, Hibbert B, and Davis DR. Systematic review of pre-clinical therapies for post-operative atrial fibrillation. *PLoS One.* 2020;15(11):e0241643.
44. McRae C, Kapoor A, Kanda P, Hibbert B, and Davis DR. Systematic review of biological therapies for atrial fibrillation. *Heart Rhythm.* 2019;16(9):1399-407.

45. Backs J, Backs T, Neef S, Kreusser MM, Lehmann LH, Patrick DM, et al. The delta isoform of CaM kinase II is required for pathological cardiac hypertrophy and remodeling after pressure overload. *Proc Natl Acad Sci U S A.* 2009;106(7):2342-7.
46. Hudmon A, and Schulman H. Structure-function of the multifunctional Ca2+/calmodulin-dependent protein kinase II. *Biochem J.* 2002;364(Pt 3):593-611.
47. Kreusser MM, Lehmann LH, Keranov S, Hoting MO, Oehl U, Kohlhaas M, et al. Cardiac CaM Kinase II genes delta and gamma contribute to adverse remodeling but redundantly inhibit calcineurin-induced myocardial hypertrophy. *Circulation.* 2014;130(15):1262-73.
48. Mesubi OO, Rokita AG, Abrol N, Wu Y, Chen B, Wang Q, et al. Oxidized CaMKII and O-GlcNAcylation cause increased atrial fibrillation in diabetic mice by distinct mechanisms. *J Clin Invest.* 2021;131(2).
49. Chelu MG, Sarma S, Sood S, Wang S, van Oort RJ, Skapura DG, et al. Calmodulin kinase II-mediated sarcoplasmic reticulum Ca2+ leak promotes atrial fibrillation in mice. *J Clin Invest.* 2009;119(7):1940-51.
50. Oort RJv, McCauley MD, Dixit SS, Pereira L, Yang Y, Respress JL, et al. Ryanodine Receptor Phosphorylation by Calcium/Calmodulin-Dependent Protein Kinase II Promotes Life-Threatening Ventricular Arrhythmias in Mice With Heart Failure. *Circulation.* 2010;122(25):2669-79.
51. Voigt N, Li N, Wang Q, Wang W, Trafford AW, Abu-Taha I, et al. Enhanced sarcoplasmic reticulum Ca2+ leak and increased Na+-Ca2+ exchanger function underlie delayed afterdepolarizations in patients with chronic atrial fibrillation. *Circulation.* 2012;125(17):2059-70.
52. Reyes Gaido OE, Pavlaki N, Granger JM, Mesubi OO, Liu B, Lin BL, et al. An improved reporter identifies ruxolitinib as a potent and cardioprotective CaMKII inhibitor. *Sci Transl Med.* 2023;15(701):eabq7839.

53. Yan J, Bare DJ, DeSantiago J, Zhao W, Mei Y, Chen Z, et al. JNK2, a Newly-Identified SERCA2 Enhancer, Augments an Arrhythmic [Ca(2+)](SR) Leak-Load Relationship. *Circ Res.* 2021;128(4):455-70.
54. Fakuade FE, Steckmeister V, Seibertz F, Gronwald J, Kestel S, Menzel J, et al. Altered atrial cytosolic calcium handling contributes to the development of postoperative atrial fibrillation. *Cardiovasc Res.* 2021;117(7):1790-801.
55. Kukielka GL, Smith CW, Manning AM, Youker KA, Michael LH, and Entman ML. Induction of interleukin-6 synthesis in the myocardium. Potential role in postreperfusion inflammatory injury. *Circulation.* 1995;92(7):1866-75.
56. Kubin T, Poling J, Kostin S, Gajawada P, Hein S, Rees W, et al. Oncostatin M is a major mediator of cardiomyocyte dedifferentiation and remodeling. *Cell Stem Cell.* 2011;9(5):420-32.
57. Friedrichs K, Baldus S, and Klinke A. Fibrosis in Atrial Fibrillation - Role of Reactive Species and MPO. *Front Physiol.* 2012;3:214.
58. Rudolph V, Andrie RP, Rudolph TK, Friedrichs K, Klinke A, Hirsch-Hoffmann B, et al. Myeloperoxidase acts as a profibrotic mediator of atrial fibrillation. *Nat Med.* 2010;16(4):470-4.
59. Yoo S, Aistrup G, Shiferaw Y, Ng J, Mohler PJ, Hund TJ, et al. Oxidative stress creates a unique, CaMKII-mediated substrate for atrial fibrillation in heart failure. *JCI Insight.* 2018;3(21).
60. Purohit A, Rokita AG, Guan X, Chen B, Koval OM, Voigt N, et al. Oxidized Ca(2+)/calmodulin-dependent protein kinase II triggers atrial fibrillation. *Circulation.* 2013;128(16):1748-57.
61. Wagner S, Dybkova N, Rasenack EC, Jacobshagen C, Fabritz L, Kirchhof P, et al. Ca2+/calmodulin-dependent protein kinase II regulates cardiac Na+ channels. *J Clin Invest.* 2006;116(12):3127-38.
62. Neef S, Dybkova N, Sossalla S, Ort KR, Fluschnik N, Neumann K, et al. CaMKII-dependent diastolic SR Ca2+ leak and elevated diastolic Ca2+ levels in right atrial myocardium of patients with atrial fibrillation. *Circ Res.* 2010;106(6):1134-44.

63. Wang Y, Li Q, Tao B, Angelini M, Ramadoss S, Sun B, et al. Fibroblasts in heart scar tissue directly regulate cardiac excitability and arrhythmogenesis. *Science.* 2023;381(6665):1480-7.
64. Alter C, Henseler AS, Owenier C, Hesse J, Ding Z, Lautwein T, et al. IL-6 in the infarcted heart is preferentially formed by fibroblasts and modulated by purinergic signaling. *J Clin Invest.* 2023;133(11).
65. Li N, and Wehrens XH. Programmed electrical stimulation in mice. *J Vis Exp.* 2010(39):e1730.

Figure 1. Single-cell landscape of poAF. (**A**) UMAP plots and (**B**) cell distributions of scRNAseq analysis of atrial non-myocytes from sham (N=3 mice, 9090 cells) and TAF (N=3 mice, 8596 cells) mice. (**C**) Macrophage annotation and (**D**) re-clustering of macrophages (n=4,946 cells) with (**E**) quantification of macrophage subtypes. (**F**) Flow cytometry with (**G**) quantification showing increased atrial $CD11b^{+}$ macrophages in TAF versus sham mice that was reversed by CL. Each dot represents one mouse. (**H**) Incidence of poAF was decreased after CL macrophage depletion. Number of mice per group is depicted. (**I**) Sample ECG tracings after atrial burst pacing. (**J**) poAF duration in Sh, TAF, and CL mice. Please note that these data show that macrophages are the most prominent cell type altered in poAF, and that macrophage depletion prevented poAF. *P*-value in (B) was obtained from chi-square test comparing the proportion of macrophages in Sham vs TAF. *P*-value in (E) was obtained from chi-square test comparing the proportion of pro-inflammatory/mixed versus non-pro-inflammatory/mixed macrophage subtypes in Sham vs TAF. *P*-values in (G) and (J) were obtained from one-way ANOVA followed by Tukey's post-hoc tests at alpha=0.05. *P*-values in (H) were obtained from chi-square tests comparing the proportion of positive poAF events. *Abbreviations*: Anti – anti-inflammatory, ANOVA – analysis of variance, B – B cell, DC – dendritic cell, EC – endothelial cell, ECG – electrocardiogram, FB – fibroblast, Mac – macrophages, Mur – mural, PMN – polymorphonuclear neutrophil, poAF – postoperative atrial fibrillation, Pro/infil – pro-inflammatory/infiltrating, Prolif– proliferating, SMC – smooth muscle cell, T – T cell, Th – thoracotomy.

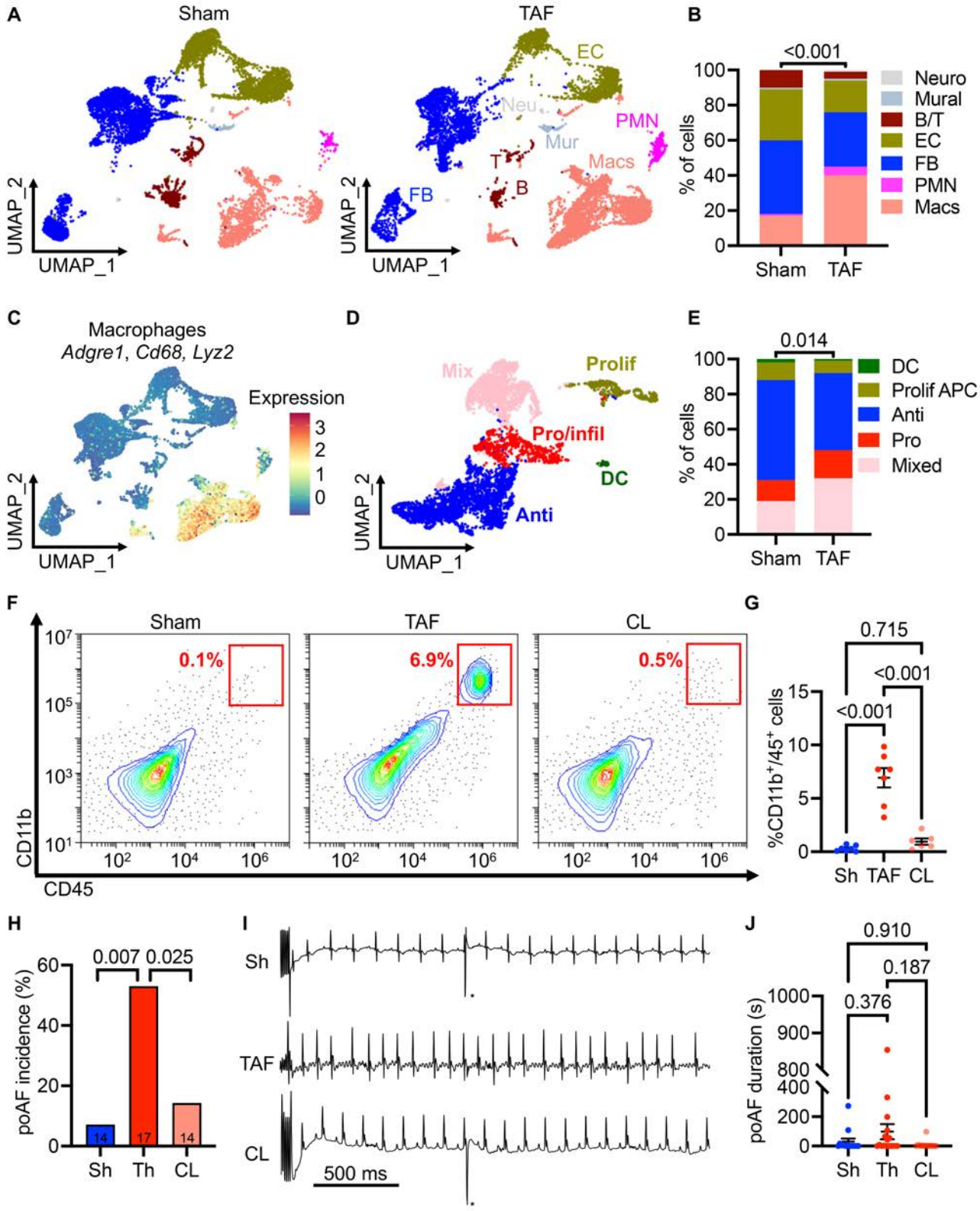
A
Sham
TAF
EC
Neu
PMN
Mur
T
Macs
B
FB
UMAP_2
UMAP_1
B
<0.001
% of cells
Neuro
Mural
B/T
EC
FB
PMN
Macs
Sham
TAF
C
Macrophages
Adgre1, Cd68, Lyz2
Expression
D
Mix
Prolif
Pro/infil
DC
Anti
E
0.014
Prolif APC
Anti
Pro
Mixed
F
Sham
TAF
CL
0.1%
6.9%
0.5%
CD11b
CD45
G
0.715
<0.001
<0.001
%CD11b+/45+ cells
Sh
TAF
CL
H
0.007
0.025
poAF incidence (%)
14
17
14
Sh
Th
CL
I
Sh
TAF
CL
500 ms
J
0.910
0.187
0.376
poAF duration (s)
Sh
Th
CL

2

Figure 2. Macrophages promote poAF through IL-6 signaling. (**A**) Monocle 3 pseudotime trajectory analyses were conducted on macrophages, (**B**) which identified *Il6*, *Il1b*, and *Socs3* as top genes changing in pseudotime. (**C**) Corresponding pseudotime-gene expression plots and (**D**) UMAP plots of the top genes changing in pseudotime. **(E)** CellChat analyses conducted using our scRNAseq dataset to identify differential cell-cell interactions in sham versus TAF mice revealed the IL-6 pathway mediated by IL-6 binding IL-6Rα and gp130 to be among the top differentially upregulated pathways. (**F**) Macrophages were the top drivers of IL-6 signaling, (**G-H**) in large part through selective expression of *Il6ra*. Please note that these data show that IL-6 is the top cytokine pathway changing in pseudotime in macrophages as well as one of the top differentially upregulated cell-cell communication pathways in TAF versus sham mice. *Abbreviations*: Adam10 – A Disintegrin and metalloproteinase domain-containing protein 10, EC – endothelial cell, FB – fibroblast, GDF – growth differentiation factor, Il1b – interleukin 1 beta, Il6 – interleukin 6, Il6ra – interleukin 6 receptor alpha, LIFR – leukemia inhibitory factor receptor, Mac – macrophage, Nlrp3 – NLR family pyrin domain containing 3, NT – neutrotrophin, PARs – proteinase activated receptors, PMN – polymorphonuclear neutrophil, Sh – sham, SLURP – secreted Ly6/uPAR-related protein, Socs3 – suppressor of cytokine signaling 3, TAF – thoracotomy atrial fibrillation

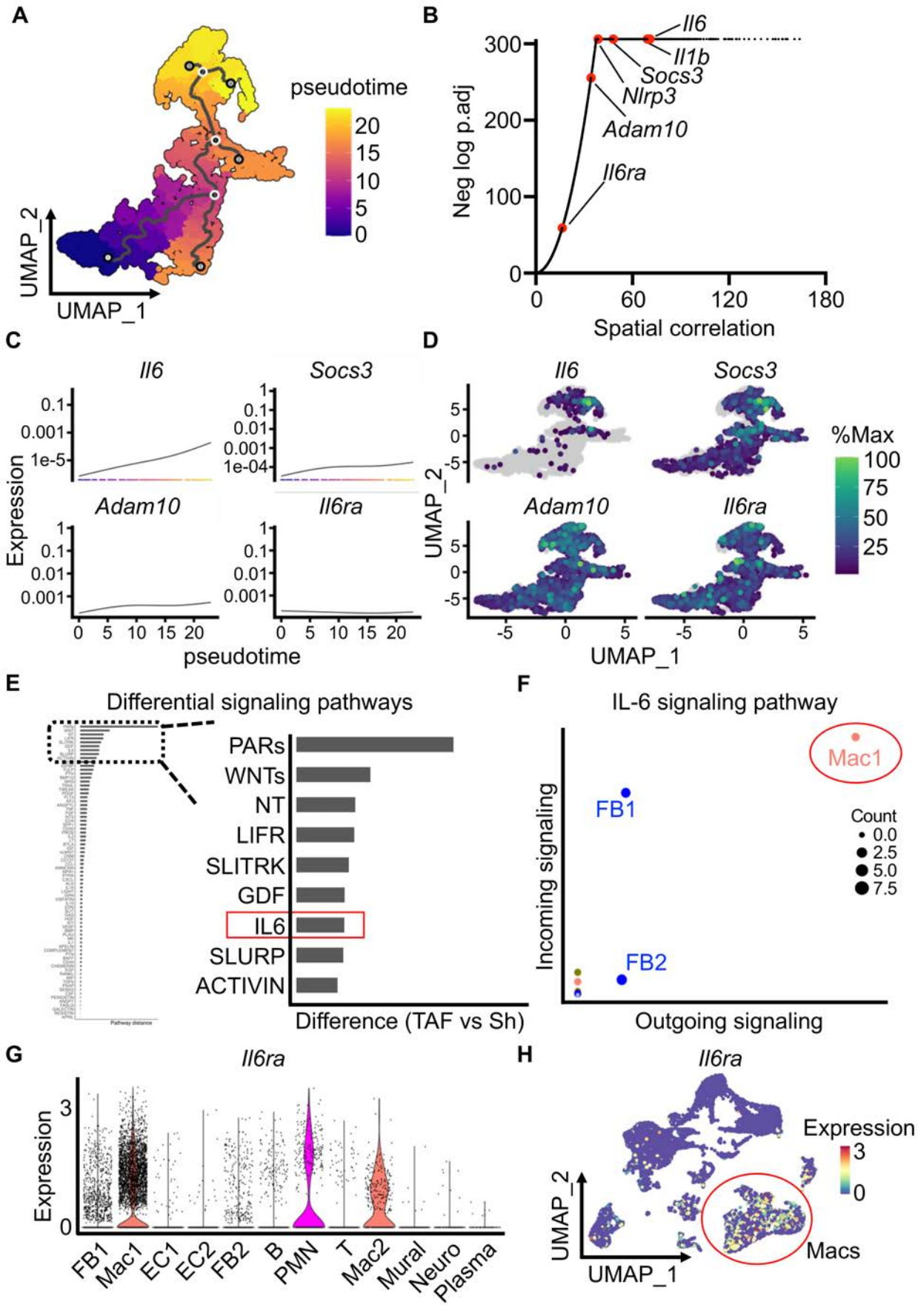
A
pseudotime
20
15
10
5
0
UMAP_2
UMAP_1
B
Il6
Il1b
Socs3
Nlrp3
Adam10
Il6ra
Neg log p.adj
300
200
100
0
0
60
120
180
Spatial correlation
C
Il6
Socs3
Adam10
Il6ra
Expression
pseudotime
D
Il6
Socs3
Adam10
Il6ra
%Max
100
75
50
25
UMAP_2
UMAP_1
E
Differential signaling pathways
PARs
WNTs
NT
LIFR
SLITRK
GDF
IL6
SLURP
ACTIVIN
Difference (TAF vs Sh)
F
IL-6 signaling pathway
Mac1
FB1
FB2
Count
0.0
2.5
5.0
7.5
Incoming signaling
Outgoing signaling
G
Il6ra
Expression
FB1
Mac1
EC1
EC2
FB2
B
PMN
T
Mac2
Mural
Neuro
Plasma
H
Il6ra
Expression
3
0
Macs
UMAP_2
UMAP_1

Figure 3. Atrial IL-6 signaling is increased in poAF. (A) Paired human PF samples collected on POD 1 and POD 3 after open-heart surgery underwent western blotting for CD68. **(B)** Western blotting of human PF samples collected on POD 3 revealed increase CD68 and IL-6 protein levels in poAF versus SR patients. Each dot in (A-B) represents one patient. (**C**) Serum IL-6 was increased in plasma from TAF compared to TSR and sham mice on POD 3. RT-qPCR from whole atria harvested on POD 3 revealed increased **(D**) *Il6* and (**E**) *Il6ra* mRNA in TAF versus TSR and sham mice. (**F**) Western blotting revealed increased IL-6 and gp130 protein levels within the atria of TAF mice. (**G**) While both greater than sham, TAF and TSR mice exhibited not exhibited differences in IL-6Rα protein levels despite greater mRNA levels, suggesting active IL-6Rα shedding in TAF mice. Each dot in (C-G) represents one mouse. Please note that these data show that macrophages and IL-6 are greater in human patients and mice with versus without poAF. *P*-value in (A) was from paired t-test. *P*-value in (B) was from two-sample t-test. *P* values in (C-G) were from one-way ANOVA followed by Tukey's post-hoc test at α=0.05. *Abbreviations*: ANOVA – analysis of variance, IL-6 – interleukin 6, IL-6Rα – interleukin 6 receptor alpha, PES – programmed electrical stimulation, PF - pericardial fluid, POD - postoperative day, SR - sinus rhythm, TAF – thoracotomy atrial fibrillation, TSR – thoracotomy sinus rhythm.

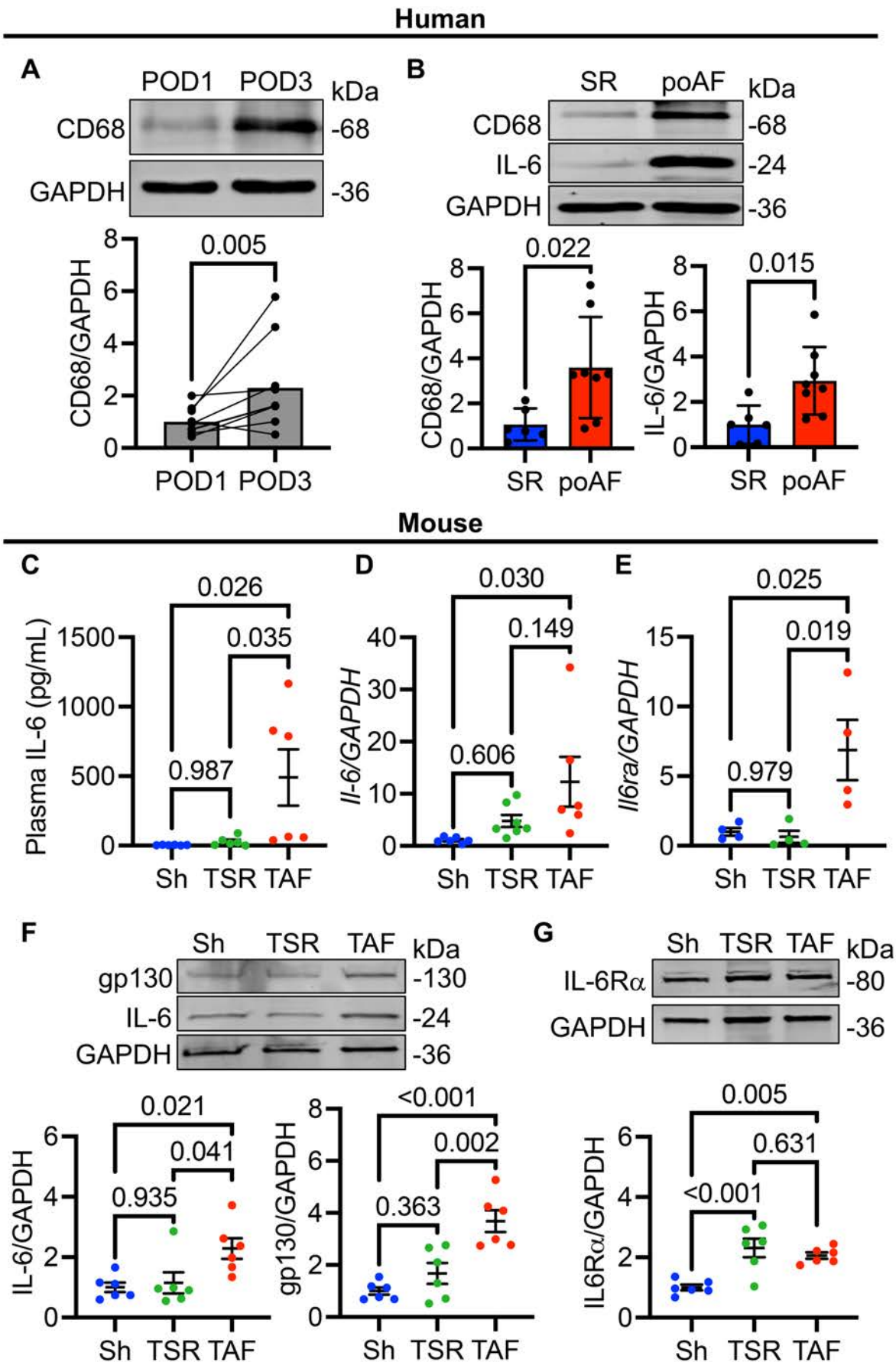
Human
A
POD1
POD3
kDa
CD68
-68
GAPDH
-36
0.005
CD68/GAPDH
POD1 POD3
B
SR
poAF
kDa
CD68
-68
IL-6
-24
GAPDH
-36
0.022
CD68/GAPDH
SR poAF
0.015
IL-6/GAPDH
SR poAF
Mouse
C
0.026
0.035
0.987
Plasma IL-6 (pg/mL)
Sh TSR TAF
D
0.030
0.149
0.606
Il-6/GAPDH
Sh TSR TAF
E
0.025
0.019
0.979
Il6ra/GAPDH
Sh TSR TAF
F
Sh
TSR
TAF
kDa
gp130
-130
IL-6
-24
GAPDH
-36
0.021
0.041
0.935
IL-6/GAPDH
Sh TSR TAF
<0.001
0.002
0.363
gp130/GAPDH
Sh TSR TAF
G
Sh
TSR
TAF
kDa
IL-6Rα
-80
GAPDH
-36
0.005
0.631
<0.001
IL6Rα/GAPDH
Sh TSR TAF

5

Figure 4. Loss of IL-6Rα from macrophages is sufficient to rescue poAF. (**A**) *Il6ra* was conditionally knocked out from macrophages by expressing Cre under the LysM promoter in *Il6ra*$^{fl/fl}$ mice. (**B-C**) Validation of *Il6rα* cKO in macrophages via flow cytometry on mouse splenocytes. Each dot represents one mouse. (**D**) Incidence of poAF was decreased in *Il6rα* cKO compared to WT mice after cardiac surgery, with decreased atrial (**E**) *Il6rα* mRNA and (**F**) protein levels. Atrial (**G**) *Il-6* and (**H-I**) pY705-STAT3 were lower in *Il6ra* cKO compared to WT mice after thoracotomy, consistent with the hypothesis that IL-6Rα from macrophages is critical for IL-6 trans-signaling in the atria. Each dot represents one mouse. Please note that these data show that selective inhibition of the IL-6 receptor in macrophages is sufficient to prevent poAF. *P*-value in (C) was obtained from a two-sample t-test. *P*-values in (D) were obtained from chi-square tests comparing the proportion of positive poAF events. *P*-values in (E-I) were obtained from one-way ANOVA followed by Tukey's post-hoc test at alpha=0.05. *Abbreviations*: ANOVA – analysis of variance, cKO – conditional knockout, IL-6Rα – interleukin 6 receptor alpha, Macs – macrophages, Sham – sham, Th – thoracotomy, TAF – thoracotomy atrial fibrillation, WT – wildtype.

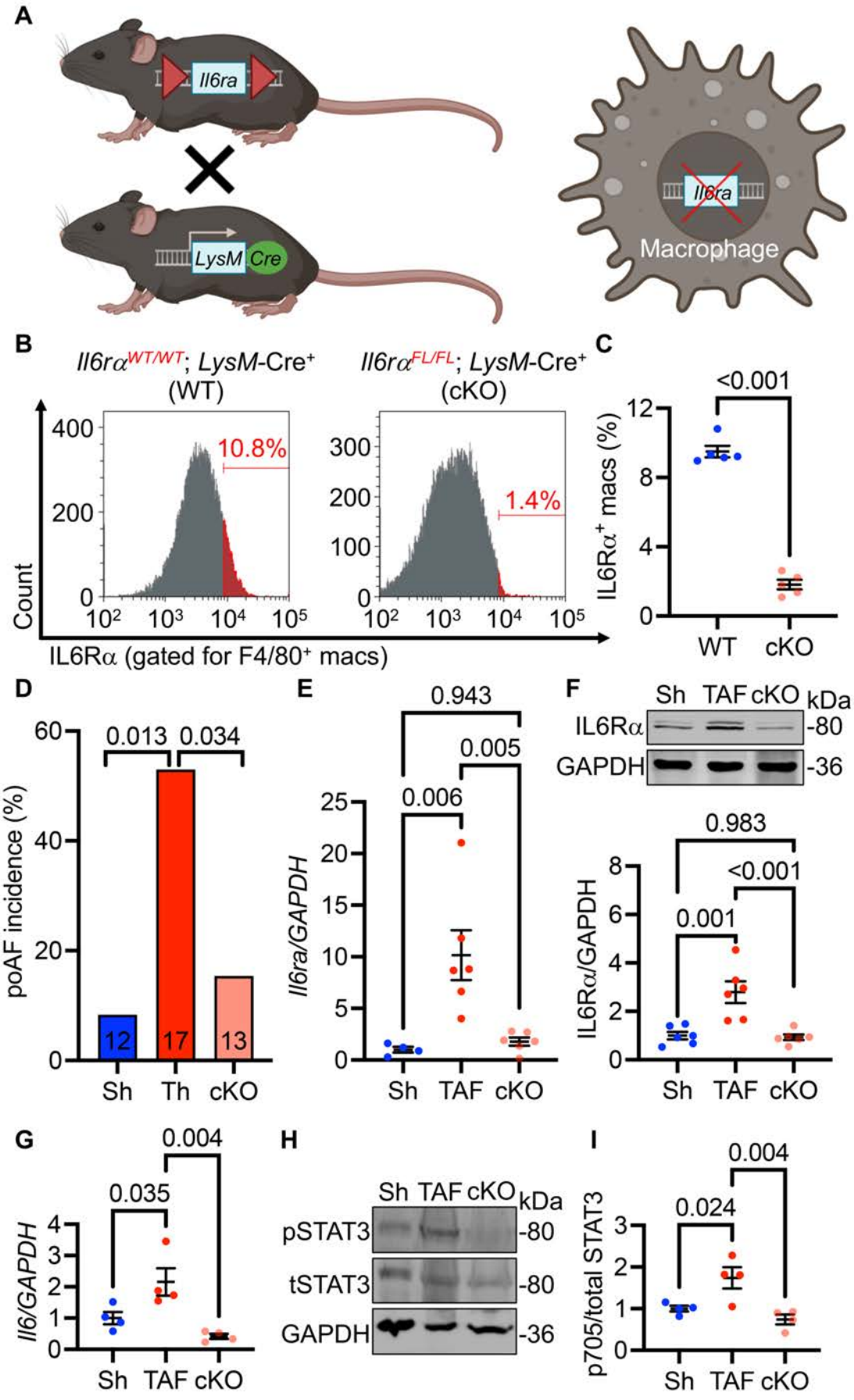
A
Il6ra
LysM Cre
Il6ra
Macrophage
B
Il6rα^WT/WT; LysM-Cre+ (WT)
Il6rα^FL/FL; LysM-Cre+ (cKO)
10.8%
1.4%
Count
IL6Rα (gated for F4/80+ macs)
C
<0.001
IL6Rα+ macs (%)
WT
cKO
D
0.013
0.034
poAF incidence (%)
12
17
13
Sh
Th
cKO
E
0.943
0.005
0.006
Il6ra/GAPDH
Sh
TAF
cKO
F
Sh TAF cKO kDa
IL6Rα
-80
GAPDH
-36
0.983
<0.001
0.001
IL6Rα/GAPDH
Sh
TAF
cKO
G
0.004
0.035
Il6/GAPDH
Sh
TAF
cKO
H
Sh TAF cKO kDa
pSTAT3
-80
tSTAT3
-80
GAPDH
-36
I
0.004
0.024
p705/total STAT3
Sh
TAF
cKO

Figure 5. STAT3-CaMKII signaling is enhanced in poAF. Western blotting revealed increased (**A**) STAT3-Y705 phosphorylation, (**B**) CaMKIIδ, and (**C**) RyR2-S2814 phosphorylation in the atria of TAF versus TSR and sham mice. (**D**) STAT3 inhibition with S3I-201 (5 mg/kg) and TTI-101 (100 mg/kg) once a day for three days (**E**) reduced poAF incidence, (**F**) with a trend towards reduced poAF duration in the TTI-101 group. (**G**) Cardiomyocyte-specific *Stat3* cKO mice (n=8) were generated by injecting AAV9-*Tnt*-Cre virus into *Stat3*$^{FL/FL}$ mice four weeks prior to cardiac surgery. Controls (n=11) consisted of mice injected with control virus four weeks prior to cardiac surgery. *Stat3* cKO mice were protected from (**H**) poAF and (**I**) exhibited a nominal reduction in poAF duration. Please note that these data show that, among mice that underwent cardiac surgery, STAT3-CaMKII-RyR2 signaling was greatest in mice that developed poAF. Pharmacologic STAT3 inhibition and cardiomyocyte-specific *Stat3* cKO prevented poAF in mice, indicating that STAT3 plays a direct pro-arrhythmogenic in cardiomyocytes. *P* values in (A-C, F) were from one-way ANOVA followed by Tukey's test for multiple correction at alpha=0.05. *P* values in (E) and (H) were from chi-square tests. *P* value in (I) was from two-sample t-test. *Abbreviations*: ANOVA – analysis of variance, CaMKIIδ – calcium/calmodulin-dependent protein kinase II delta, cKO - conditional knockout, Inj – injection, PES – programmed electrical stimulation, pRyR2 - phospho-RyR2-S2814, pSTAT3 - phospho-Tyr705-STAT3, RyR2 – ryanodine receptor 2, Sham – sham, SR – sinus rhythm, Thor – thoracotomy, TNT - troponin T, TSR – thoracotomy sinus rhythm, tSTAT3 - total STAT3, TTI – TTI-101.

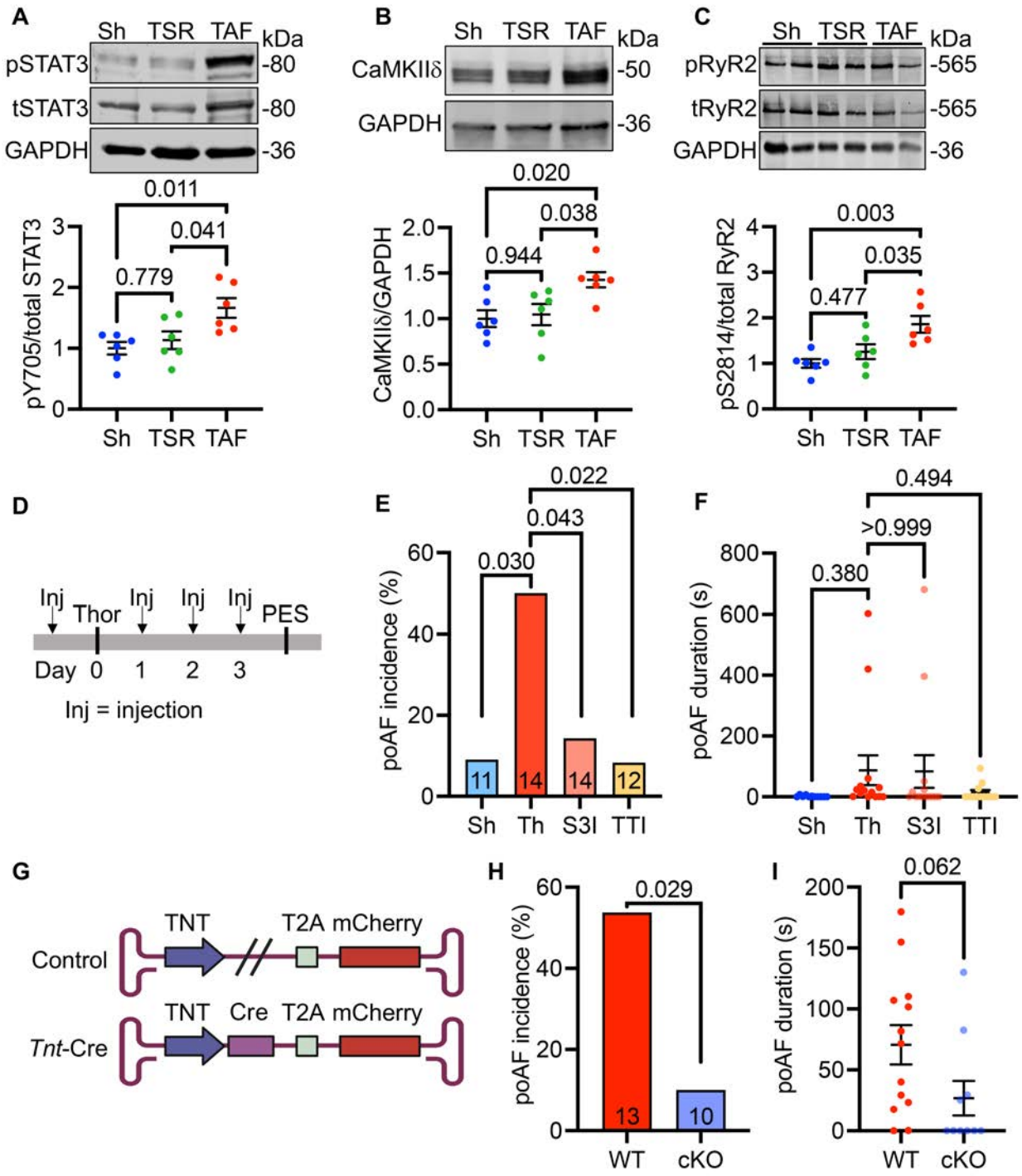
A
Sh TSR TAF kDa
pSTAT3 -80
tSTAT3 -80
GAPDH -36
0.011
0.041
0.779
pY705/total STAT3
Sh TSR TAF
B
Sh TSR TAF kDa
CaMKIIδ -50
GAPDH -36
0.020
0.038
0.944
CaMKIIδ/GAPDH
Sh TSR TAF
C
Sh TSR TAF kDa
pRyR2 -565
tRyR2 -565
GAPDH -36
0.003
0.035
0.477
pS2814/total RyR2
Sh TSR TAF
D
Inj Thor Inj Inj Inj PES
Day 0 1 2 3
Inj = injection
E
0.022
0.043
0.030
poAF incidence (%)
11 14 14 12
Sh Th S3I TTI
F
0.494
>0.999
0.380
poAF duration (s)
Sh Th S3I TTI
G
TNT T2A mCherry
Control
TNT Cre T2A mCherry
Tnt-Cre
H
0.029
poAF incidence (%)
13 10
WT cKO
I
0.062
poAF duration (s)
WT cKO

Figure 6. Optical mapping of mouse hearts in sham and thoracotomy mice. Langendorff-perfused mouse hearts from sham (n=5) and thoracotomy (n=8) mice were paced at 10 Hz, and conduction velocity and coefficient of variation were assessed in the (**A-C**) right and (**D-F**) left atria. Induction of atrial arrhythmias was assessed using an S1-S2 pacing protocol (see Supplementary Materials). Representative atrial electrograms and corresponding voltage-sensitive dye oscillations during and after S1-S2 pacing in (**G**) Sham and (**H**) Thor mice. Blue arrows in (G) and (H) denote S1 pacing at 10 Hz while red arrows denote premature stimulus (S2). Red arrowheads in (G) and (H) denote time stamps at which the images below were taken. White asterisks in paced beat image denotes location of pacing electrode (right atrium) while yellow asterisks in (H) denote triggered activity. (**I**) Atrial arrhythmia incidence, defined as >=2 positive atrial tachyarrhythmia events after S1-S2 pacing, and (**J**) the incidence of triggered activity, defined as the percent of total S1-S2 protocols that led to triggered activity, were significantly greater in thoracotomy versus sham mice. (**K**) AERP did not differ between groups. Please note that these data show that triggered activity is the primary arrhythmia mechanism in our murine poAF mouse model given the lack of reentry-driving substrate alterations. *P* values in (B-C), (E-F), and (J-K) were derived from two-sample t-tests. *P* value in (I) was derived from Fisher's exact test. *Abbreviations*: AERP - atrial effective refractory period, CoV - coefficient of variation, CV - conduction velocity, DADs - delayed afterdepolarizations, Sh - sham, SR - sinus rhythm, Th - thoracotomy.

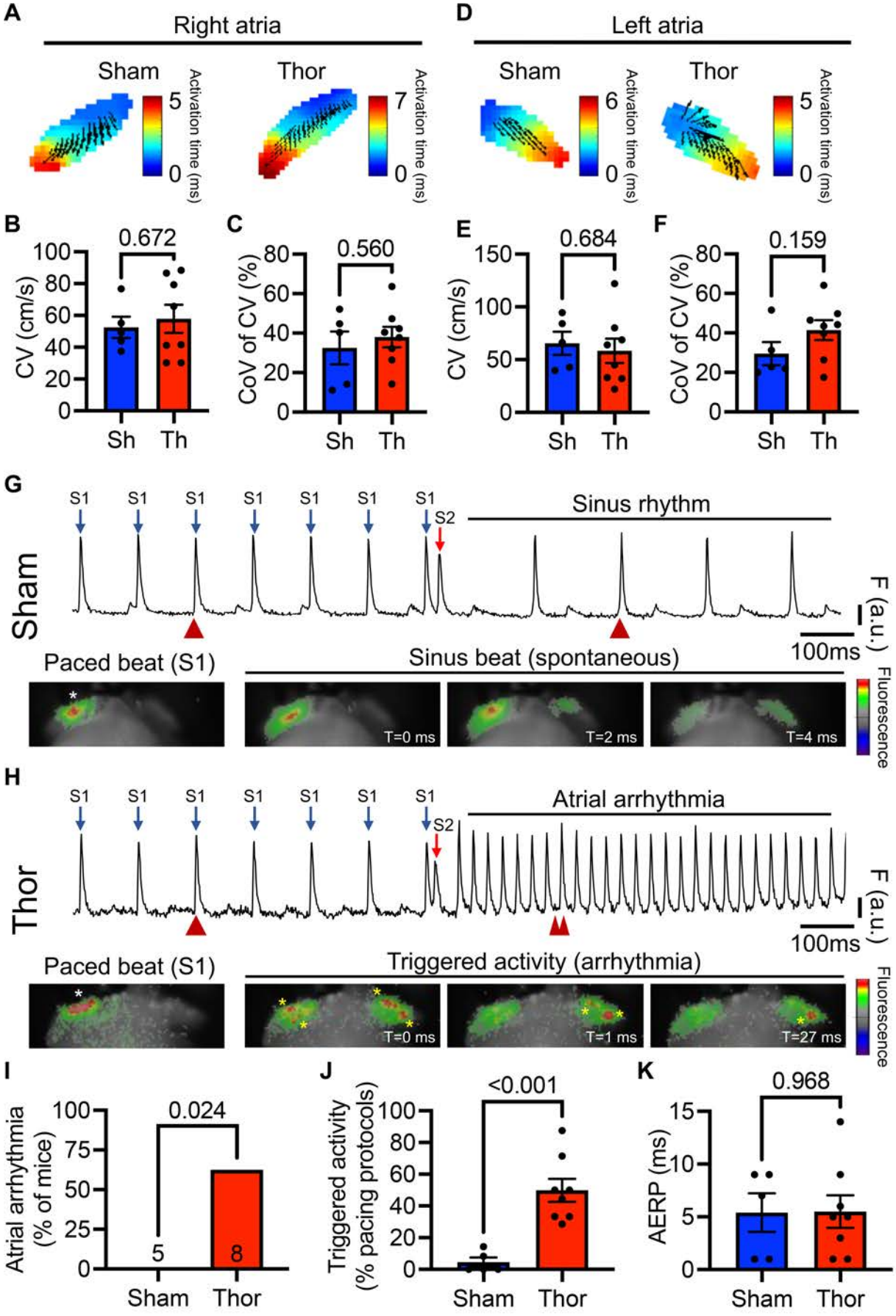
A
Right atria
Sham
Thor
Activation time (ms)
5
0
7
0
D
Left atria
Sham
Thor
6
0
5
0
B
CV (cm/s)
0.672
Sh
Th
C
CoV of CV (%)
0.560
E
0.684
F
0.159
G
Sham
S1
S2
Sinus rhythm
F (a.u.)
100ms
Paced beat (S1)
Sinus beat (spontaneous)
T=0 ms
T=2 ms
T=4 ms
Fluorescence
H
Thor
Atrial arrhythmia
Triggered activity (arrhythmia)
T=0 ms
T=1 ms
T=27 ms
I
Atrial arrhythmia (% of mice)
0.024
5
8
J
Triggered activity (% pacing protocols)
<0.001
K
AERP (ms)
0.968

Figure 7. IL-6 is sufficient to induce arrhythmogenic Ca^{2+} mishandling in ACMs. Primary wild-type mouse cardiomyocytes were incubated with IL-6 (200 ng/mL) + IL-6Rα (100 ng/mL), followed by (**A**) RT-qPCR for *Camk2d* after 30-min of treatment and (**B**) western blotting for STAT3-Y705 phosphorylation and CaMKIIδ protein after 2-h of treatment. Atrial cardiomyocytes (ACMs) isolated from WT mice were incubated with IL-6 (200 ng/mL) + IL-6Rα (100 ng/mL) or vehicle (PBS) for 1.5-h prior to confocal imaging of SR Ca^{2+} handling. (**E**) ACMs exposed to vehicle (top) or IL-6/R (bottom) were paced at 1-Hz through field stimulation, followed by a 60-s diastolic pause to assess Ca^{2+} sparks and waves prior to rapid 10 mM caffeine exposure to assess SR Ca^{2+} load. (**F**) Representative Ca^{2+} spark images obtained after the pacing train in ACMs exposed to vehicle (top) or IL-6/R (bottom). Asterisk* indicates corresponding Ca^{2+} wave in tracing (E) and spark image (F). Quantification of (**G**) paced Ca^{2+} transient amplitude, (**H**) CaSpF, (**I**) SR Ca^{2+} load, (**J**) CaSpF/SR Ca^{2+} load, and (**K**) Ca^{2+} wave incidence (cells with waves/total cells) revealing increased CaSpF, CaSpF/SR Ca^{2+} load, and waves after IL-6/R treatment. Number of mice and ACMs are denoted under each figure panel. *P*-values in (A-D) were obtained from two-sample t-tests. *P*-values in (G-J) were from nested t-tests to account for clustering of data by mouse and treatment group. *P* value in (K) was from chi-square test. *Abbreviations*: Ca^{2+} - calcium ion, CaSpF – calcium spark frequency, CaT – calcium transient, IL-6/R – interleukin-6 + interleukin-6 receptor alpha, SR – sarcoplasmic reticulum, TAF – thoracotomy atrial fibrillation.

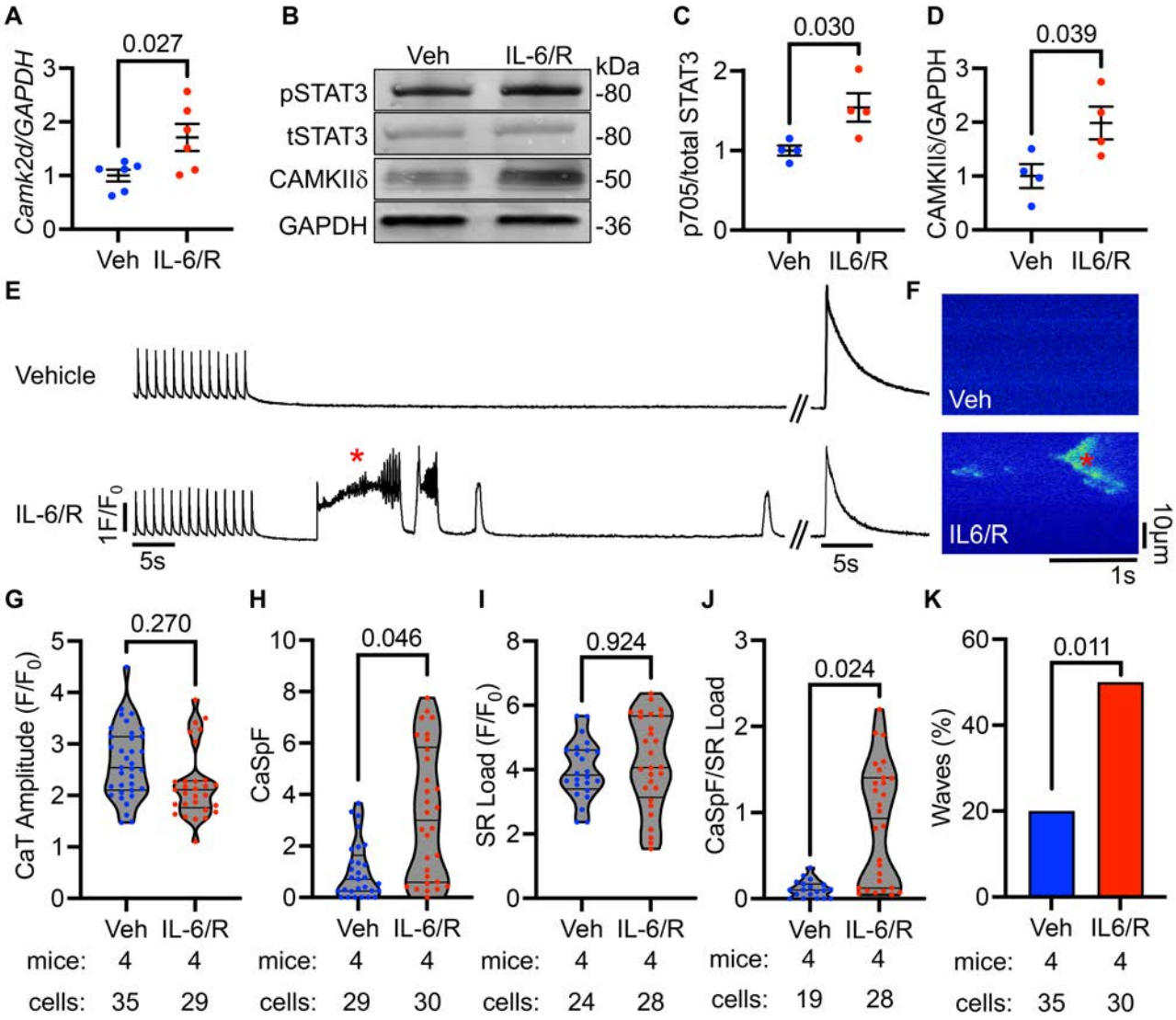
A
0.027
Camk2d/GAPDH
Veh
IL-6/R
B
Veh
IL-6/R
kDa
pSTAT3
tSTAT3
CAMKIIδ
GAPDH
-80
-80
-50
-36
C
0.030
p705/total STAT3
Veh
IL6/R
D
0.039
CAMKIIδ/GAPDH
Veh
IL6/R
E
Vehicle
IL-6/R
1F/F0
5s
5s
F
Veh
IL6/R
10μm
1s
G
0.270
CaT Amplitude (F/F0)
Veh
IL-6/R
mice: 4 4
cells: 35 29
H
0.046
CaSpF
Veh
IL-6/R
mice: 4 4
cells: 29 30
I
0.924
SR Load (F/F0)
Veh
IL-6/R
mice: 4 4
cells: 24 28
J
0.024
CaSpF/SR Load
Veh
IL-6/R
mice: 4 4
cells: 19 28
K
0.011
Waves (%)
Veh
IL6/R
mice: 4 4
cells: 35 30

8

Figure 8. CaMKII inhibition rescues Ca^{2+} mishandling in poAF. ACMs were isolated from sham, TSR, and TAF mice. A subgroup of ACMs from TAF mice were pretreated with CaMKII inhibitor KN-93 for 30 minutes prior to confocal Ca^{2+} imaging. (**A**) Representative diastolic Ca^{2+} spark images after 1-Hz field pacing of ACMs isolated from Sh, TSR, TAF, and TAF ACMs pretreated with KN-93. Quantification of (**B**) CaSpF, (**C**) SR Ca^{2+} load, (**D**) CaSpF/SR Ca^{2+} load, and **(E)** spontaneous Ca^{2+} wave incidence. Next, non-phosphorylatable *RyR2*^{S2814A}, phosphomimetic *RyR2*^{S2814D} mice, and WT littermates underwent sham or thoracotomy. (**F**) Incidence of poAF, (**G**) number of poAF events, and (**H**) poAF duration were decreased in *RyR2*^{S2814A} compared to WT mice. Please note that these data show TAF ACMs have greater arrhythmogenic Ca^{2+} sparks and waves compared to TSR and that CaMKII inhibition is sufficient to reverse these changes. Indeed, CaMKII phosphorylation at RyR2-S2814 is a necessary action of CaMKII in poAF as *RyR2*^{S2814A} were protected from poAF. *P*-values in (B-E) were from nested 1-way ANOVA to account for clustering of data by mouse and treatment group. *P* value in (F) was from chi-square test. *P* value in (H) was from one-way ANOVA followed by Tukey's test to correct for multiple testing at α=0.05. *Abbreviations*: Sh - sham, TSR - thoracotomy sinus rhythm, TAF - thoracotomy atrial fibrillation, Thor - thoracotomy.

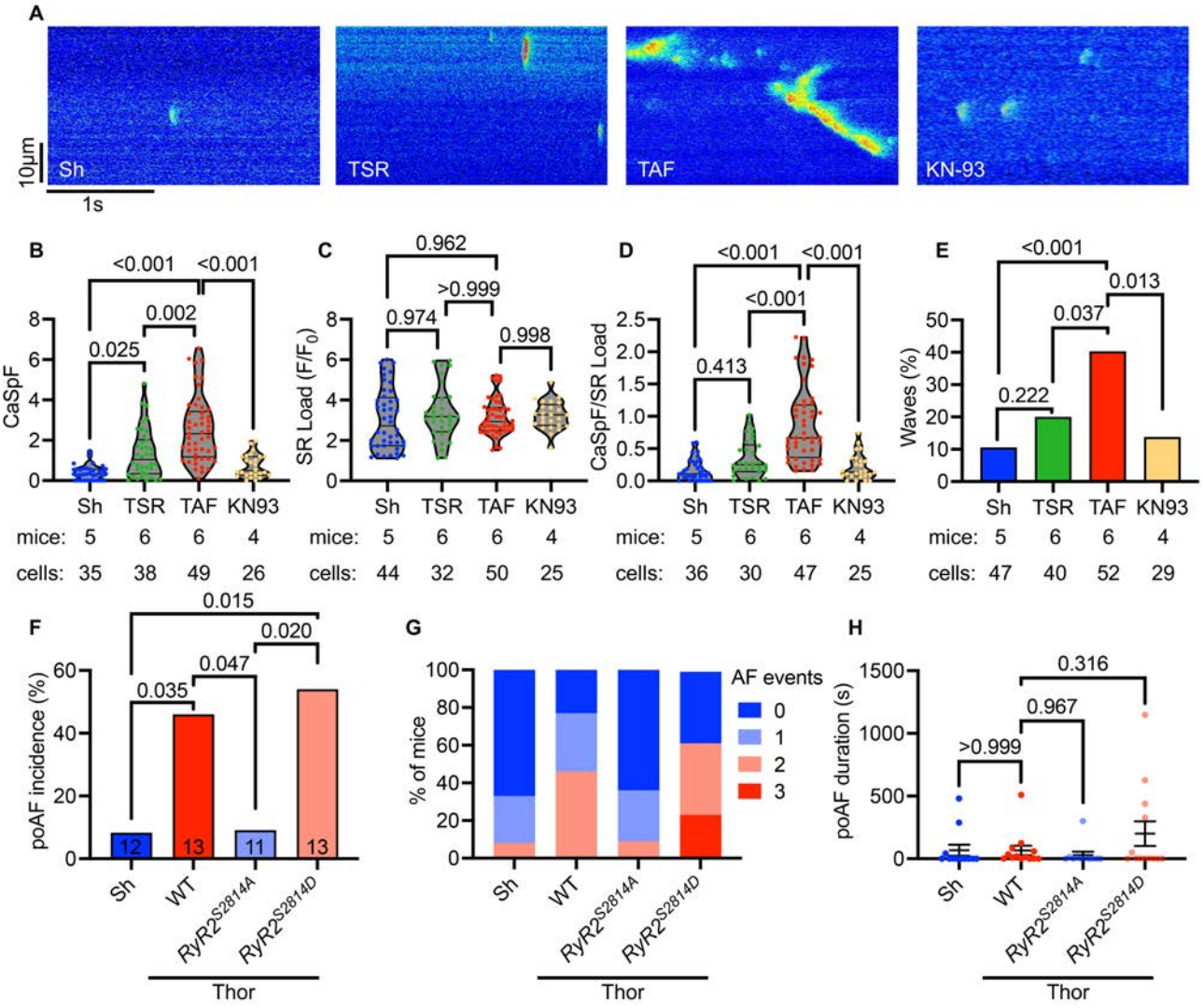
A
10µm
1s
Sh
TSR
TAF
KN-93
B
CaSpF
<0.001
<0.001
0.002
0.025
Sh TSR TAF KN93
mice: 5 6 6 4
cells: 35 38 49 26
C
SR Load (F/F0)
0.962
>0.999
0.974
0.998
Sh TSR TAF KN93
mice: 5 6 6 4
cells: 44 32 50 25
D
CaSpF/SR Load
<0.001
<0.001
<0.001
0.413
Sh TSR TAF KN93
mice: 5 6 6 4
cells: 36 30 47 25
E
Waves (%)
<0.001
0.013
0.037
0.222
Sh TSR TAF KN93
mice: 5 6 6 4
cells: 47 40 52 29
F
poAF incidence (%)
0.015
0.020
0.047
0.035
12
13
11
13
Sh
WT
RyR2S2814A
RyR2S2814D
Thor
G
% of mice
AF events
0
1
2
3
Sh
WT
RyR2S2814A
RyR2S2814D
Thor
H
poAF duration (s)
0.316
0.967
>0.999
Sh
WT
RyR2S2814A
RyR2S2814D
Thor

4

Table 1. Mouse PES parameters.

	Sham (n=14)		Thor (n=17)		Thor + CL (n=14)		*P*
	Mean±SEM	**IQR (range)**	**Mean±SEM**	**IQR (range)**	**Mean±SEM**	**IQR (range)**	
RR	128.8±4.15	21 (61)	126.4±2.88	32 (38.4)	124.0±4.55	25 (59)	0.700
PR	43.3±1.03	2.1 (12.1)	44.7±0.90	6.7 (10.9)	44.5±1.82	10.9	0.720
QRS	14.1±0.20	1.3 (2.5)	14.5±0.35	2.7 (4.2)	15.1±0.93	1.7 (2.9)	0.071
SNRT	178.2±13.95	66 (194)	156.5±6.04	36 (102)	163.2±10.16	53 (129)	0.309
AVERP	48.7±1.52	6.5 (24)	50.6±2.08	8.0 (38)	55.9±7.24	9.0 (30)	0.460
	Sham (n=12)		**Thor (n=17)**		***Il6rα* cKO (n=13)**		***P***
	Mean±SEM	**IQR (range)**	**Mean±SEM**	**IQR (range)**	**Mean±SEM**	**IQR (range)**	
RR	128.0±5.65	37 (58)	132.0±4.08	26 (64)	126.0±4.13	31 (46)	0.624
PR	42.9±1.42	5.7 (19.2)	44.2±0.59	3.0 (10.1)	46.2±1.02	5.5 (14)	0.094
QRS	13.9±0.27	1.2 (3.0)	14.1±0.26	1.7 (3.3)	13.8±0.16	0.80 (2.1)	0.578
SNRT	146.9±8.77	43 (98)	158.1±8.58	59 (109)	165.9±10.5	29 (131)	0.401
AVERP	51.3±2.50	15 (30)	53.1±1.57	7.0 (30)	48.9±1.67	9.0 (20)	0.267
	Sham (n=11)		**Thor (n=14)**		**Thor + S3I (n=14)**		**Thor + TTI (n=12)**		***P***
	Mean±SEM	**IQR (range)**	**Mean±SEM**	**IQR (range)**	**Mean±SEM**	**IQR (range)**	**Mean±SEM**	**IQR (range)**	
RR	138.4±5.17	20 (59)	128.5±3.99	17 (57)	123.9±3.79	23 (53)	129.3±5.13	30 (53)	0.172
PR	45.0±0.64	3.0 (7.5)	45.0±0.93	3.1 (14)	44.0±0.93	6.0 (11.7)	43.6±0.79	3.0 (11)	0.596
QRS	14.0±0.33	1.3 (4.2)	13.8±0.28	1.6 (3.3)	14.3±0.37	1.4 (5.8)	13.5±0.24	1.2 (3.0)	0.384
SNRT	183.6±12.52	47 (148)	166.9±8.29	35 (109)	152.6±8.14	34 (110)	163.9±9.27	26 (93)	0.174
AVERP	54.8±1.12	6.5 (10)	52.2±2.21	7.5 (28)	53.3±1.38	8.5 (18)	49.7±2.45	10 (32)	0.311

	Sham (N=12)		Thor (WT, N=13)		Thor (*RyR2*^{S2814A}, N=11)		Thor (*RyR2*^{S2814D}, N=13)		*P*
	Mean±SEM	**IQR (range)**	**Mean±SEM**	**IQR (range)**	**Mean±SEM**	**IQR (range)**	**Mean±SEM**	**IQR (range)**	
RR	136±3.67	21 (44)	125±3.80	24 (44)	119±3.44	23 (33)	121±5.45	27 (66)	0.039
PR	44.7±1.29	7.0 (13)	45.5±0.77	5.5 (8.4)	44.9±0.80	3.3 (9.5)	46.4±1.04	6.9 (10)	0.612
QRS	13.9±0.32	1.3 (3.8)	14.1±0.16	0.70 (2.1)	13.8±0.26	1.7 (2.4)	14.4±0.24	1.5 (2.5)	0.440
SNRT	199±25.5	123 (267)	148±10.3	60 (117)	153±9.1	58 (86)	190±16.9	114 (165)	0.065
AVERP	50.7±1.99	10 (20)	49.7±2.16	10.5 (26)	47.1±1.60	7.0 (16)	47.5±2.19	6.0 (30)	0.556

Electrocardiographic parameters from mouse PES studies. Values displayed in ms as mean (SEM). *P* values were obtained from one-way ANOVA. *Abbreviations*: ANOVA - analysis of variance, AVERP - atrioventricular nodal effective refractory period, CL - clodronate liposome, ms - millisecond, IQR - interquartile range, PES - programmed electrical stimulation, SEM - standard error of the mean, SNRT - sinus node recovery time, Thor - thoracotomy, TTI - TTI-101.